

# Hijacking the Neuronal NMDAR Signaling Circuit to Promote Tumor Growth and Invasion

Leanne Li<sup>1</sup> and Douglas Hanahan<sup>1,\*</sup>

<sup>1</sup>Swiss Institute for Experimental Cancer Research, School of Life Science, Swiss Federal Institute of Technology Lausanne (EPFL), Lausanne 1015, Switzerland

\*Correspondence: douglas.hanahan@epfl.ch

<http://dx.doi.org/10.1016/j.cell.2013.02.051>

## SUMMARY

Glutamate and its receptor N-methyl-D-aspartate receptor (NMDAR) have been associated with cancer, although their functions are not fully understood. Herein, we implicate glutamate-driven NMDAR signaling in a mouse model of pancreatic neuroendocrine tumorigenesis (PNET) and in selected human cancers. NMDAR was upregulated at the periphery of PNET tumors, particularly invasive fronts. Moreover, elevated coexpression of NMDAR and glutamate exporters correlated with poor prognosis in cancer patients. Treatment of a tumor-derived cell line with NMDAR antagonists impaired cancer cell proliferation and invasion. Flow conditions mimicking interstitial fluid pressure induced autologous glutamate secretion, activating NMDAR and its downstream MEK-MAPK and CaMK effectors, thereby promoting invasiveness. Congruently, pharmacological inhibition of NMDAR in mice with PNET reduced tumor growth and invasiveness. Therefore, beyond its traditional role in neurons, NMDAR may be activated in human tumors by fluid flow consequent to higher interstitial pressure, inducing an autocrine glutamate signaling circuit with resultant stimulation of malignancy.

## INTRODUCTION

Invasion and metastasis is a defining hallmark in the pathogenesis of most forms of human cancer (Hanahan and Weinberg, 2011; Nguyen et al., 2009). Metastasis is a major cause of cancer morbidity, and invasiveness contributes both to metastatic dissemination as well as to locally invasive tumor growth with concomitant tissue damage. The limited efficacy of most conventional and targeted anticancer therapies may relate in part to their largely ineffectual inhibition of cancer progression via invasion and metastasis.

Previously our laboratory identified an invasion modifier locus on chromosome 17 in the RIP1-Tag2 transgenic mouse model of pancreatic neuroendocrine tumorigenesis (PNET) (Chun et al.,

2010). Within this locus, an N-Methyl-D-aspartate receptor (NMDAR)-associated gene, *dlgap1*, was one of several candidate proinvasive genes selectively upregulated in invasive carcinomas. We were led, therefore, to consider the potential involvement of the NMDAR in PNET tumorigenesis, especially in invasion.

NMDAR is a receptor governing synaptic plasticity in the CNS, where it plays important roles in learning, memory, and neuron maturation. NMDARs have also been detected in various human tumor samples and cell lines, and patch-clamp experiments in several cancer cell lines have demonstrated receptor functionality (Stepulak et al., 2009). However, the functional importance of NMDAR signaling in cancers is unclear. Notably, the mechanistic contributions and pathologic significance of NMDAR activation in elaborating cancer phenotypes are poorly understood (Prickett and Samuels, 2012).

Glutamate, the major physiological agonist of the NMDAR, has long been implicated in cancer (Rzeski et al., 2001). A role in promoting tumor growth and invasion was first established in glioma (Takano et al., 2001). Subsequently, an increasing number of cancer cells have been found to secrete glutamate (Seidlitz et al., 2009; Sharma et al., 2010) although the effector mechanisms and functional importance of secreted glutamate remain elusive. Glutamate is a ligand for two classes of receptors that are either G protein coupled or ion channels; NMDAR is a member of the ionotropic class. Protumoral effects of glutamate have been attributed to its signaling via G-protein-coupled glutamate receptors (Nicoletti et al., 2007) or via the AMPA receptor (Herner et al., 2011), another ionotropic glutamate receptor; in contrast, there is little evidence implicating glutamate signaling via NMDAR in cancer phenotypes. Motivated by these various considerations, we sought to determine whether the NMDAR and its ligand glutamate might be involved in invasive growth in the mouse model of PNET and, if so, to investigate the regulation and mechanistic effects of NMDAR signaling in such tumors and the possible translational relevance to human cancer.

## RESULTS

### NMDAR Is Upregulated in Genetically Engineered Mouse Models of Cancer

The RIP1-Tag2 line of transgenic mice presents a genetically engineered mouse model (GEMM) of human PNET (Hanahan,

1985). We found that both subunits of the heterodimeric NMDAR, namely NR1 (Figure S1 available online) and NR2b (Figure 1A), were expressed in PNETs arising in this model. NR2b expression was elevated toward the tumor periphery (Figures 1A and 1B, i), particularly at invasion fronts (Figure 1C). The increased NR2b expression at the tumor periphery was evident in 96.6% of PNETs examined (Figure 1B, i), and the elevation of NR2b expression toward the tumor periphery was more evident as tumor size increased (Figure 1B, ii). Moreover, NR2b phosphorylation at Y1252, which enhances NMDAR activity (Takasu et al., 2002), was more pronounced at the tumor periphery than in the tumor center (Figure 1D). We also examined the expression of NMDAR in mouse models of pancreatic ductal adenocarcinoma (PDAC) (Grippio and Tuveson, 2010) and breast cancer (Fantozzi and Christofori, 2006). NR2b was also variably upregulated at the tumor periphery or in invasive cells in these GEMMs (Figures 1E–1G and Table S1). Although the RIP1-Tag2 model is highly synchronized, presenting with discrete tumors as a function of age that renders them easily quantifiable, both the breast and PDAC models are temporally and histologically heterogeneous, with merged lesions of varying tumor grades noted in late stage disease. Thus we were not able to quantify the patterns of NMDAR expression in these two GEMMs.

#### **NMDAR Pathway Is Evident in Multiple Human Cancers and Is Associated with Poor Cancer Patient Prognosis**

Having documented the elevated expression of NMDAR in several GEMMs of human cancer, we next audited NMDAR expression using human tissue microarrays (TMA). High NR2b expression was noted in some samples from pancreatic ductal carcinoma (Figure S2A), breast cancer (Figures 2A and 2B), ovarian cancer (Figure 2C), and glioma (Figure 2E), but not in others (Table S2). In the breast cancer TMA, we found that high NR2b expression was associated with the HER2 subtype, whereas negative NR2b expression was observed more in the luminal subtype (Figures 2A and S2B), suggesting that NR2b had different expression patterns among different subtypes. Interestingly, one patient sample in the breast cancer TMA expressed an intermediate to high level of NR2b and showed invasion into adjacent adipose tissues (Figure 2B), whereas a paired sample from the same patient in the same TMA, which was not immediately adjacent to the invasion fronts, expressed only low level of NR2b (Figure 2B).

Glutamate is the major agonist for NMDAR. In neurons, vesicular glutamate transporters (vGlut1, -2, and -3) export glutamate to initiate signaling. Thus we assessed vGlut expression in conjunction with NMDAR for possible association with cancer patient survival in the TCGA database. In our survey of human cancer, TMAs we had found overexpression of NR2b in glioma (Figure 2E) and in ovarian cancer (Figure 2C). When we segregated glioblastoma (grade 4 glioma) patients by levels of both NR2b and vGlut2 into higher and lower expressing groups (see Extended Experimental Procedures), the difference was striking: the median survival was 4.4 months longer in the vGlut2/NR2b-low group, reaching 15.2 months as compared to 10.8 months for the vGlut2/NR2b-high group (Figures 2F and S2D). Notably, vGlut1 and vGlut3 levels had a similar correlation (Figure S2D).

We also analyzed the ovarian cancer data set in TCGA and found a similar trend: the median survival was one year longer in the NR2b/vGlut2-low expression group than in the high expression group (Figures 2D and S2C). In contrast, in the TCGA lung squamous cell carcinoma data set, low versus high expression of NR2b/vGluts was not associated with differential patient prognosis (Figure S2E), suggesting, quite reasonably, that not all tumor types are affected by variable levels of NMDAR.

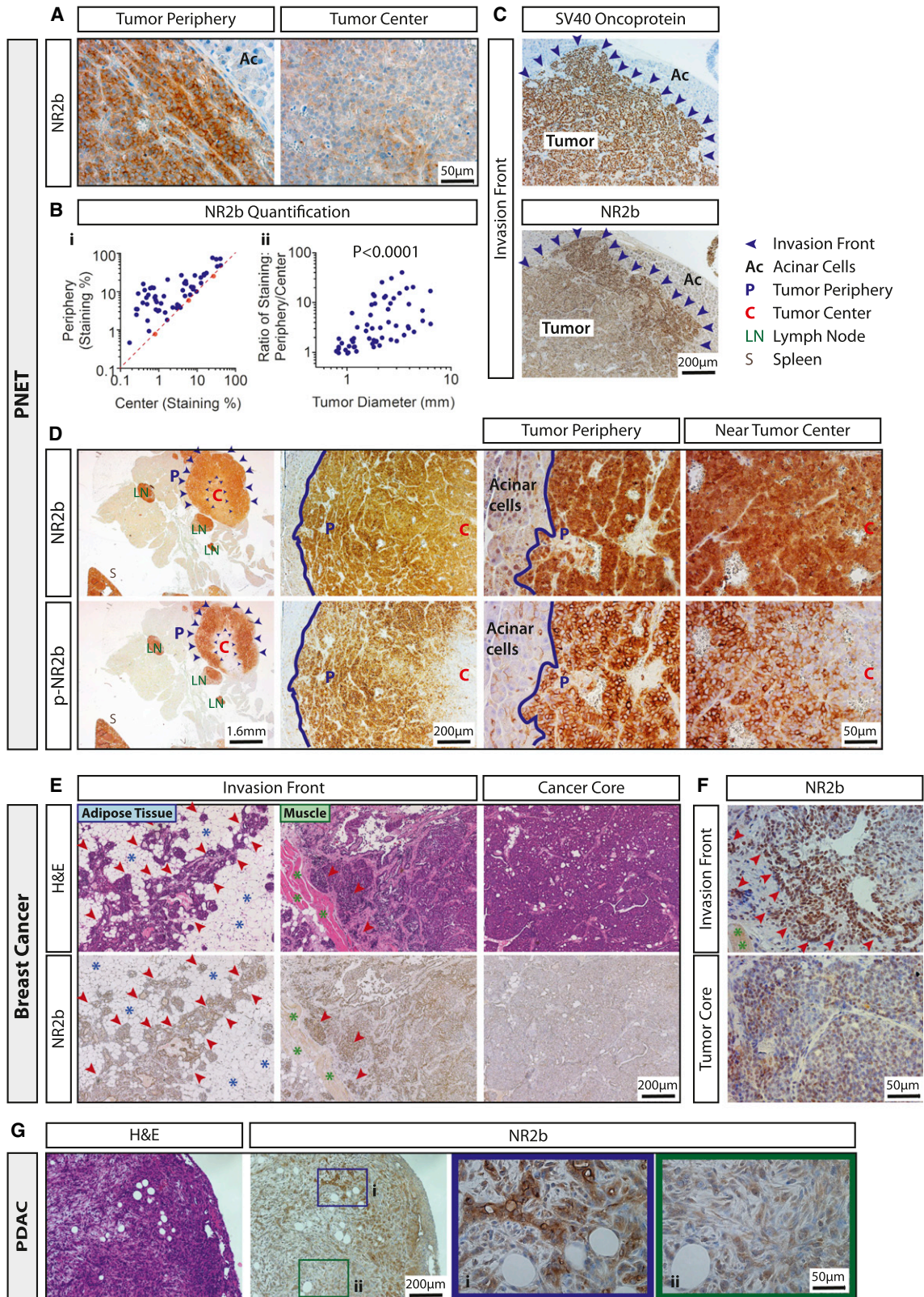
#### **Inhibiting NMDAR Has Antiproliferative and Anti-Invasive Effects In Vitro**

Motivated by our observations that the NMDAR was expressed at elevated levels in various human cancer types compared to cognate normal tissues and that patients whose tumors had comparatively higher levels had worse prognosis, we returned to the mouse PNET model to investigate possible roles of NMDAR signaling in this form of cancer. First, we employed the  $\beta$ TC-3 cancer cell line, derived from a PNET tumor in a RIP1-Tag2 mouse (Efrat et al., 1988), to investigate the potential involvement of NMDAR in cancer cell phenotypes in vitro. We used an NMDAR antagonist, MK801, to study the possible contributions of NMDAR—via its inhibition—on proliferation and apoptosis. MK801 is a selective, noncompetitive NMDAR inhibitor. MK801 blocks the calcium channel of the NR1 subunit with high affinity; as such it is one of the most potent known NMDAR antagonists. We applied MK801 to cultures of  $\beta$ TC-3 cancer cells and observed a time-dependent decrease in proliferation and increase in apoptosis (Figure 3A).

In our previous experience, cultured PNET cancer cells (exemplified by the  $\beta$ TC-3 cell line) are weakly invasive in the traditional transwell invasion assay (Du et al., 2007). Therefore, we employed a modified invasion assay developed by Swartz and colleagues (Shields et al., 2007) (Figures 3B and S3), which uses hydrostatic pressure to create a mimetic of interstitial fluid pressure and consequent fluid flow. As compared to the traditional static invasion assay, the flow-based invasion assay (Figure 3B) significantly increased  $\beta$ TC-3 invasiveness, which could be blocked by MK801, indicating a substantive role for NMDAR in cancer cell invasion in this ex vivo assay (Figure 3C). Because AMPAR, another glutamate receptor, has previously been implicated in promoting cancer invasion (Herner et al., 2011), we also examined the effect of an AMPAR antagonist—GYKI52466—in the flow-based invasion assay. Modest anti-invasive activity was observed, albeit much weaker than that of MK801 (Figure 3C).

To verify that these were not off-target effects of MK801, we knocked down the obligatory NMDAR subunit NR1 in  $\beta$ TC-3 cells and found that NR1 siRNA phenocopied the effects of the NMDAR inhibitor MK801 on cancer cell survival and invasiveness (Figure 3D).

In our TMA survey, both pancreatic adenocarcinomas (Figure S2A) and breast cancers (Figures 2A and 2B) were found to express NR2b. Therefore, we performed some of the key in vitro experiments on a panel of human breast and pancreatic cancer cell lines that covered a variety of different subtypes (Table S3). Varying responses in terms of reduced cell survival (Figure 3E) and (flow-guided) invasion (Figure 3F) were noted in MK801-treated groups. Notably, the effect of MK801 on



(legend on next page)

invasiveness was in general more pronounced than on survival. When the tested cell lines were divided into three groups according to their invasiveness in the modified invasion assay, we found that within both highly and moderately invasive groups, the response to MK801 correlated with NR2b mRNA expression (Figure 3G). In contrast, NR2b was barely detectable in the weakly invasive group, and in this group the treatment response was instead associated with NR2a expression (Figure 3G). Interestingly, there was no association between the level of NR2b or other NMDAR subunits and reduced cell survival upon treatment with MK801 (data not shown). Overall, the results suggest that elevated levels of NR2b expression are particularly deterministic for flow-mediated invasion.

### NMDAR Signaling in PNET Is Autologous and Can Be Activated by Interstitial Flow

In light of demonstrating that NMDAR signaling was enhancing the cancer cell phenotypes of proliferation and invasiveness in conditions mimicking interstitial pressure-driven flow, we sought to assess the possible involvement of its ligand glutamate in regulating such phenotypes.

By analyzing mRNA isolated from different stages of PNET tumorigenesis using qRT-PCR, we found increased vGlut gene expression in the solid tumor stage, as compared to normal pancreatic islets and premalignant stages (Figures 4A and S4A). This result is consistent with previous studies showing that vGluts are not expressed in normal mouse islet  $\beta$  cells but are detectable and fully functional in  $\beta$ TC-6 (Bai et al., 2003), another PNET cell line derived from the RIP1-Tag2 mouse model (Poitout et al., 1995). Notably, the expression level varied considerably among tumors, as shown by the floating bars covering minimum to maximum values (Figure 4A). This observation is indicative of heterogeneous activation of NMDAR signaling among PNETs, consistent with the considerable range of NR2b staining in different tumors (Figure 1B).

To pinpoint the cellular sources of glutamate, we used fluorescence-activated cell sorting (FACS) to separate PNETs into their different constituent cell types. In neurons, classical paracrine NMDAR signaling involves presynaptic neurons expressing

vGluts that mediate glutamate secretion to stimulate postsynaptic neurons expressing the glutamate receptor NMDAR, as well as glial cells (and sometimes neurons) expressing EAATs (excitatory amino-acid transporters) that remove extracellular glutamate to modulate NMDAR signaling. By qRT-PCR, we identified cancer cells as the major expressers of all three components of this signaling loop (Figures 4B and S4B), indicative of autocrine NMDAR signaling. We also examined another glutamate transporter, xCT, and found it to be highly expressed by infiltrating immune (inflammatory) cells (Figure S4B). Therefore, paracrine glutamate signaling from immune inflammatory cells to the cancer cells might be operative in PNETs as well.

vGlut family proteins were also expressed in the  $\beta$ TC-3 cancer cell line (Figure 4C), and immunostaining showed a typical punctate localization of vGlut3 in the cytoplasm (Figure 4D). The finding that the glutamate transporters and NMDAR were coexpressed in  $\beta$ TC-3 cancer cells led us to investigate whether autocrine glutamate secretion was involved in their capability for invasion. Our initial experiments revealed that  $\beta$ TC-3 invasiveness was enhanced by hydrostatic flow (Figure 3C). Congruently, we found increased levels of glutamate in medium conditioned by  $\beta$ TC-3 cancer cells in flow conditions (Figure 4E), consistent with interstitial flow enhancing glutamate secretion and autocrine signaling via NMDAR in PNET cancer cells.

### Interstitial Flow Promotes NMDAR Surface Localization

Having determined that autologous glutamate secretion was enhanced under the flow conditions that promoted  $\beta$ TC-3 invasion in the modified invasion assay, we added glutamate to the traditional (static) invasion assay. Interestingly, adding glutamate could not fully recapitulate the degree of invasiveness seen in the flow-based invasion assay (data not shown). Therefore, the following question emerged: in addition to increasing the levels of secreted ligand, might interstitial flow be directly affecting the glutamate receptor NMDAR?

We used flow cytometry to analyze NMDAR surface expression in regular 2D-cultured (static)  $\beta$ TC-3 cancer cells and found heterogeneous surface expression of both NR1 and NR2b (Figure S5A), which was also observed by immunostaining

### Figure 1. Involvement of NMDAR Signaling in Genetically Engineered Mouse Models of Cancer—Descriptive Evidence

(A) In the RIP1-Tag2 mouse model of pancreatic neuroendocrine tumors (PNET), expression of the NMDAR subunit 2b (NR2b) is selectively elevated at tumor periphery as compared to tumor center (images were taken from the same tumor).

(B) Semiquantification of NR2b expression in mouse PNETs. (i) A pair of images was taken from each tumor analyzed, one from the center and the other from the periphery. Image pairs from 59 PNETs excised from nine mice were digitally quantified for NR2b staining intensity (as described in the [Extended Experimental Procedures](#)), which revealed that NR2b was in most tumors significantly overexpressed at the periphery. Only three out of 59 tumors (spots marked in red) fell under the red dashed-line (slope = 1) representing equal level of staining at the periphery and center. (ii) Using the data from (i), a ratio for each tumor was generated by dividing the average staining intensity for NR2B at the tumor periphery with that of the center. This ratio of overexpression was positively associated with tumor diameter measured on semithin tissue sections (nonparametric correlation, two-tailed Spearman's test, with  $r_s = 0.6621$ ).

(C) NR2b overexpression was particularly evident at invasion fronts; immunostaining for the oncoprotein expressed by the transgenic RIP1-Tag oncogene reveals the cancer cells.

(D) Phospho-NR2b, indicative of signaling activity, was also preferentially detected at the tumor periphery; a transition from positive to equivocal/negative staining was observed in fields near the tumor center.

(E) In the MMTV-PyMT mouse model of breast cancer, increased NR2b expression was observed in cancer cells invading into adipose tissues and muscle layers compared to those at the tumor core. (Blue asterisks, adipocytes; green asterisks, muscle layer; red arrow heads, invading cancer cells).

(F) High magnification of breast cancer cells invading into the muscle layer showed elevated NR2b staining compared to cells in the tumor core. (Green asterisks, muscle layer; red arrow heads, invading cancer cells).

(G) In a mouse model of pancreatic ductal adenocarcinoma (PDAC), a similar trend of NR2b overexpression at the tumor periphery (i) compared to the tumor center (ii) was also noted.

See also [Figure S1](#) and [Table S1](#).

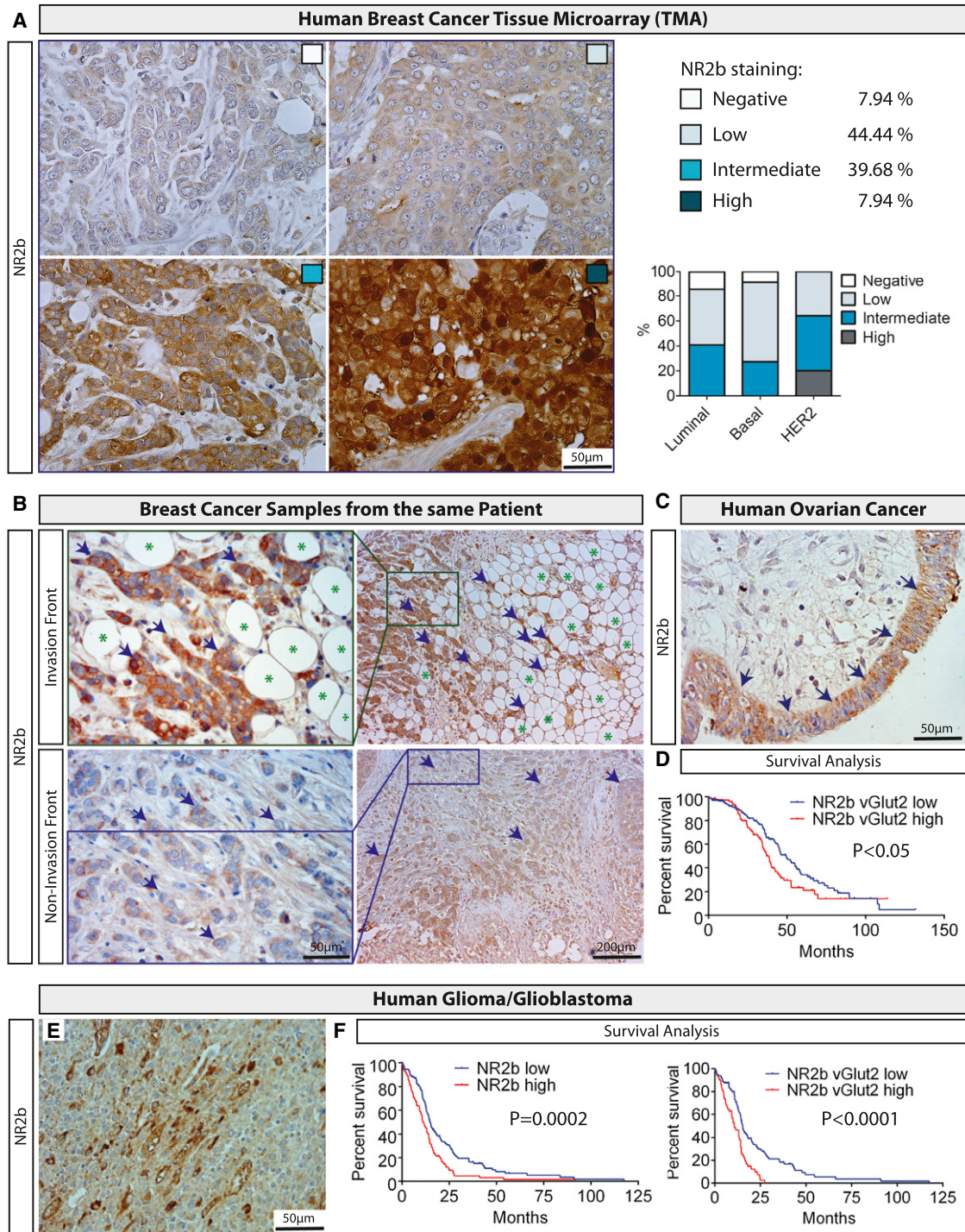


**Figure 2. Involvement of NMDAR Signaling in Human Cancers—Descriptive Evidence**

(A) A nonexhaustive survey involving human cancer tissue microarrays (TMA) revealed varying intensity of NR2b staining in the tumor samples. The staining intensity was categorized into four levels: negative, low, intermediate, and high. The percentage of each category from the TMA was documented. Interestingly, NR2b staining was associated with different breast cancer subtypes.  $p < 0.05$ , Chi-square test.

(B) In one patient sample in the TMA, breast cancer cells with intermediate to high level of NR2b expression were invading into the adjacent adipose tissue, whereas a paired sample that was not immediately adjacent to an invasive front showed negative to low levels of NR2b expression. (Green asterisks, adipocytes; blue arrows, cancer cells).

(C) Example from a similar analysis of an ovarian cancer TMA, which also revealed elevated NR2b expression in a subset of cancer cells. (Blue arrow: ovarian cancer cells).

(legend continued on next page)

(Figure S5B). However, when we stained for both surface and intracellular NMDARs, uniform levels of NR1 and NR2b were detected (Figure S5A). This result suggested that there was an intracellular pool of NMDARs primed for surface recruitment in response to appropriate signals, similar to the situation in neurons (Lau and Zukin, 2007). This observation suggested that interstitial flow might be involved in regulating the surface expression of NMDAR. Indeed, flow cytometry analysis revealed that the levels of the two NMDAR subunits on the cell surface were increased in flow conditions as compared to the static condition (Figure 5A). Thus interstitial flow modulates surface localization of NMDAR as well as glutamate secretion.

### Interstitial Flow Activates the CaMK and MEK-MAPK Pathways Downstream of NMDAR

Ligand-stimulated NMDAR induces calcium influx in neurons, which activates two major downstream signaling circuits: the  $\text{Ca}^{2+}$ /calmodulin kinase (CaMK) pathway and the MEK-MAPK pathway (Hardingham and Bading, 2010); both lead to phosphorylation of the transcription factor CREB (cAMP response element-binding protein) at Ser133 (Figure 5B), a prerequisite for recruiting the transcriptional coactivator CREB-binding protein (CBP) to the promoter regions of effector genes.

To clarify which pathway(s) downstream of NMDAR is involved in cancer cell invasion, we analyzed phosphoprotein expression in  $\beta$ TC-3 cancer cells in the invasion assay. We found that interstitial flow increased NR2b phosphorylation (Figure 5C), which is known to potentiate NMDAR activity (Takasu et al., 2002) and to promote NR2b surface localization (Braithwaite et al., 2006) in neurons. We also observed increased phosphorylation of calmodulin kinase type II (CaMK-II), calmodulin kinase type IV (CaMK-IV), MAPK/ERK kinase (MEK), and p44/p42 mitogen-activated protein kinase (MAPK) in flow conditions as compared to static conditions, leading to a modest increase in CREB phosphorylation at Ser133 (Figure 5C). Consistent with our hypothesis that NMDAR mediates flow-activated signaling, the addition of the NMDAR antagonist MK801 to the flow-stimulated invasion assay markedly decreased the phosphorylation of these effector proteins, with the exception of CAMK-IV (Figure 5C). Strikingly, pretreatment with BAPTA-AM, a potent intracellular calcium chelator commonly used to block intracellular calcium signaling, in particular calcium-dependent NMDAR signaling (Marsden et al., 2007), was able to abolish flow-induced protein phosphorylation of all these effectors in both MEK-MAPK and CAMK pathways, including CAMK-IV (Figures 5D and S5D). The results establish that the flow-mediated activation of the CaMK and MEK-MAPK pathways is calcium-dependent, principally involving the calcium-dependent NMDAR.

### In Vivo the NMDAR Antagonists Have Therapeutic Efficacy

Having characterized NMDAR signaling in assays involving cultured cancer cells, we proceeded to perform experimental therapeutic trials in the RIP1-Tag2 mouse model in order to assess the importance of NMDAR signaling for tumors in vivo.

The synchronized, multistage tumorigenesis pathway to PNET in RIP1-Tag2 mice renders this GEMM a powerful tool for experimental trials of mechanism-targeted drugs. By 12–14 weeks of age, 2%–4% of the approximately 400 pancreatic islets have progressed through premalignant stages to become solid tumors with varying degrees of invasiveness (Chun et al., 2010), and the mice reach end stage at around 14–16 weeks. Several distinctive experimental trial regimens have proved informative about the molecular, histological, and pathological effects of anticancer drugs: intervention trials start at 10–11 weeks of age and last 3–4 weeks, aiming to determine if a drug can intervene in the expansive growth of nascent solid tumors; regression trials start at 12–13 weeks, to assess a drug's effect when substantial solid tumors have developed, and the mice are at a late stage of disease progression (Bergers et al., 1999). Regression trials in this mouse model therefore mimic a common situation in the clinic, when treatment commences in patients with advanced solid tumors.

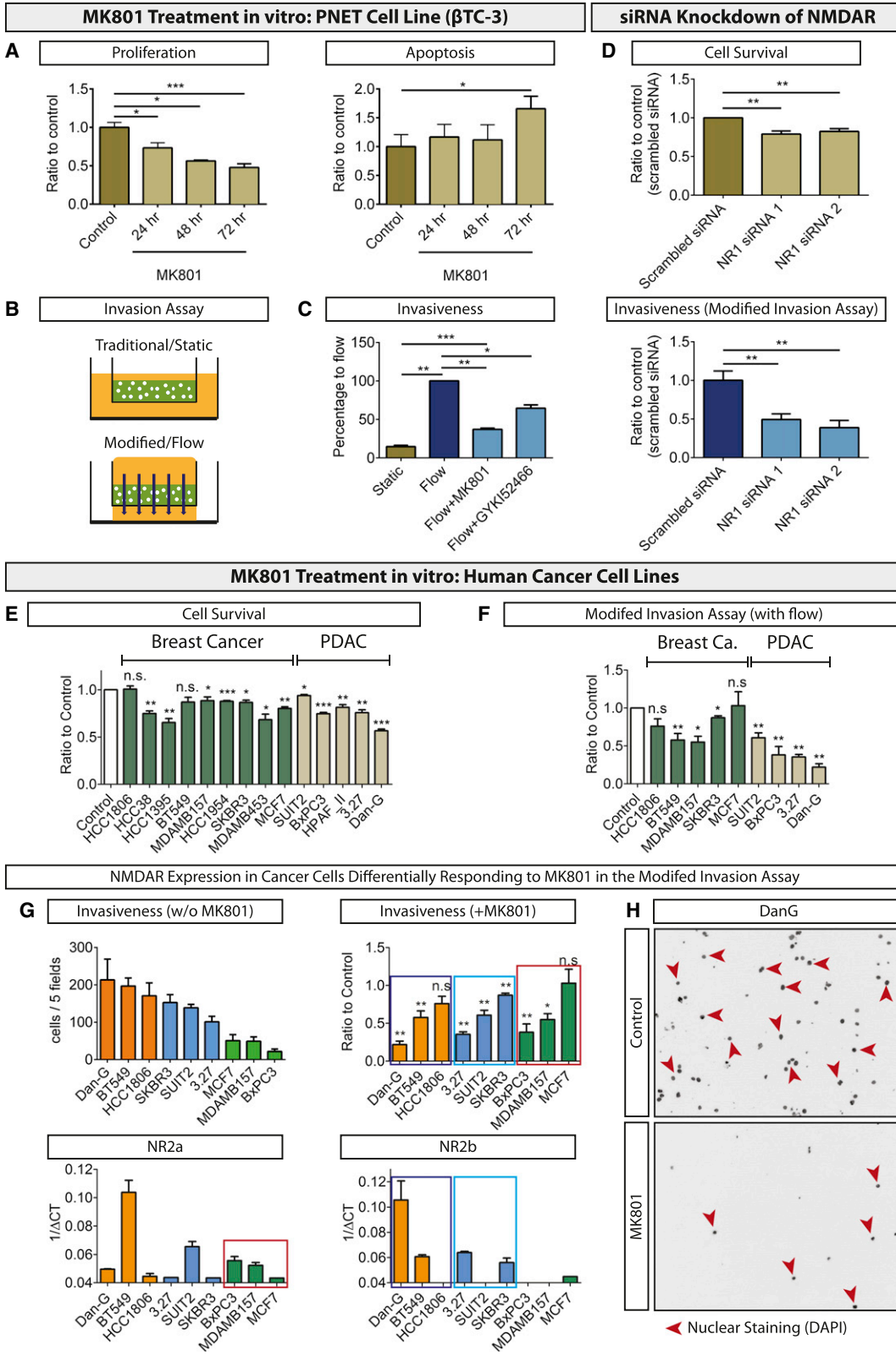
In an intervention trial with MK801, tumor burden (cumulative volume of multiple tumors in the pancreas) and tumor number were both decreased by the treatment (Figure 6A), concomitant with reduced proliferation (Figure 6B). Tumor invasiveness was also attenuated (Figure 6A). In addition, NR2b expression and phosphorylation at the tumor periphery were decreased in MK801-treated tumors (Figure 6B). We then performed a regression trial, and found that MK801 was even more effective in decreasing tumor burden at this late stage of progression (Figure 6C). We also tested a much weaker, clinically approved NMDAR antagonist, memantine, and observed an antitumoral effect in the late stage regression trial, but not in the early stage intervention trial (Figure S6A), perhaps reflecting its weaker activity. We then performed a preclinical trial with MK801 in a second mouse model, involving orthotopic transplantation of primary breast cancer cells from MMTV-PyMT transgenic mice. After 3 weeks of treatment, we observed a trend toward decreased tumor burden (Figure S6B); we infer that the lack of statistical significance reflects similar heterogeneity in NMDAR expression to what we described above both in breast tumors in the GEMM and in patient samples (by immunohistochemistry and mRNA profiling). Collectively, the preclinical trials support the implications from the analysis of clinical data that NMDAR signaling is functionally important in some tumor types (Figure S2 and Tables S1 and S2) and that individual tumors of particular

(D) Querying the TCGA database of ovarian cancer patients for the combination of NR2b and the glutamate transporter vGlut2 revealed that a group with low expression levels of both NR2b and vGlut2 (below mean) had more than one year of survival advantage compared to a distinctive NR2b/vGlut2 high group (above mean). Median survival, 49.4 months in NR2b/vGlut2 low group; 36.9 months in NR2b/vGlut2 high group.

(E) NR2b was also expressed in samples from a glioma TMA, as exemplified by one tumor.

(F) Survival analysis using glioblastoma patient data in the TCGA data set revealed that NR2b expression levels alone were significantly associated with prognosis (median survival, 14.9 months in NR2b low group versus 11.5 months in NR2b high group). Moreover, the combination of low versus high levels of NR2b plus vGlut2 further separated the curves (median survival, 15.2 months in NR2b/vGlut2 low group versus 10.8 months in NR2b/vGlut2 high group).

See also Figure S2 and Table S2.



cancer types and subtypes could have heterogeneous expression and consequently variable responses to MK801 treatment (Figure 3E).

## DISCUSSION

The results presented herein provide provocative evidence for a functional role of the NMDAR signaling pathway in tumor progression. In addition, they unveil a mechanism of NMDAR pathway activation in cancer: physical cues in cancer microenvironment, namely interstitial pressure differences and fluid flow, serve to activate an autocrine pathway that stimulates proliferation and invasiveness of cancer cells (Figure 7).

### Glutamate Is Subject to Flow-Regulated Secretion for Autocrine Stimulation of NMDAR

We have revealed a mechanism that regulates glutamate bioavailability in the tumor microenvironment, demonstrating that during tumorigenesis, glutamate bioavailability and signaling are evidently elevated by three mechanisms. First, the vGlut genes are transcriptionally upregulated in the cancer cells. Second, increased interstitial pressure and flow in the microenvironment elicit increased glutamate secretion by those cancer cells. Third, flow conditions increase both expression and cell-surface localization of the glutamate receptor NMDAR so as to enable stronger signaling in response to the glutamate ligand. Concordantly, the combination of higher expression of NR2b and vGluts was predictive of poor prognosis for cancer patients.

### Interstitial Flow as a Microenvironmental Signal

Deciphering the complex crosstalk between cancer cells and their microenvironment stands as an important challenge to the cancer field (Hanahan and Weinberg, 2011). Among the various environmental parameters, cancer-associated stromal cells are prominent, and their importance is increasingly well established (Hanahan and Coussens, 2012). In contrast, invisible cues, such as the physical forces within the tumor microenvironment, have been less well studied and appreciated. Recently, mechanotransduction has begun to emerge as an

instructor for cancer progression (DuFort et al., 2011). Elevated tumor interstitial fluid pressure (IFP) and consequently increased interstitial flow have been associated with tumor invasion and lymph node metastasis (Shieh and Swartz, 2011) and with poor patient prognosis (Heldin et al., 2004). Interstitial flow is typically highest at tumor margins due to the differential interstitial fluid pressure between tumor and adjacent normal tissue (Dafni et al., 2002; Harrell et al., 2007). Congruently, as demonstrated in Figure 5, flow conditions increased both surface expression of NMDAR and NR2b phosphorylation and enhanced invasion by PNET cancer cells, consistent with the observation that NR2b expression and NR2b phosphorylation preferentially occurred at the periphery of PNET tumors (Figures 1A–1D). Moreover, IFP and interstitial flow are known to increase significantly as tumor size increases (Gutmann et al., 1992), consistent with our observation that peripherally elevated expression of NR2b was positively associated with tumor size (Figure 1B, ii). Notably, the therapeutic benefit of the NMDAR inhibitors MK801 and memantine are much more significant in the late stage regression trial than in the early stage intervention trial (Figures 6A, 6C, and S6A), again implicating the preferential activation of NMDAR in late stage tumors via increased interstitial pressure and consequent flow, leading to heightened malignancy.

### Proliferation and Invasion May Be Governed by Distinct Branched Pathways Downstream of NMDAR

In the in vitro assay, the anti-invasive effect of MK801 (evident within overnight culture) occurred much faster than its antiproliferative and proapoptotic effects (evident after 3 days) on cancer cells in vitro (Figures 3A and 3C). This result suggests that NMDAR-mediated invasion might involve different downstream effectors than those that modulate survival. The analysis of protein phosphorylation in the invasion assay (Figure 5C) provides some insights into the downstream pathways of NMDAR.

By comparing cells in flow conditions with those in flow plus MK801 conditions, we could attribute the observed reductions in invasion by MK801 in flow conditions (Figure 5C) to the

### Figure 3. Functional Importance of NMDAR Signaling in Cancer—In Vitro Evidence

- (A) Treating cultured PNET cancer cells with the NMDAR antagonist MK801 decreased proliferation and increased apoptosis.  
 (B) Schematic of the modified invasion assay that mimics interstitial fluid pressure-mediated pressure gradients and fluid flow.  
 (C) In the modified invasion assay shown in (B), flow significantly increased cancer cell invasiveness, which could be inhibited both by the NMDAR antagonist MK801 and (to a lesser extent) by the AMPAR antagonist GYKI52466.  
 (D) The invasion- and growth-inhibiting effects of MK801 could be recapitulated with siRNA-mediated knockdown of the obligatory NMDAR subunit 1 (NR1).  
 (E and F) Treatment of a panel of human breast and PDAC cancer cell-lines with MK801 variably reduced cell survival (E), and invasiveness using the modified invasion assay (F).  
 (G) Out of the 14 cell lines shown in (E), 9 cell lines were selected for evaluation of NR2a/b mRNA expression. The 9 cell lines could be divided into three groups according to their invasiveness: high (DanG, BT549, HCC1806), intermediate (SKBR3, SUI7, 3.27), and weak (MCF7, MDAMB157, BxPC3). Interestingly, NR2b expression was associated with the response to MK801 within high and intermediate invasiveness groups. NR2b was barely detectable in the weakly invasive group; instead, MK801's effects on invasion were associated with differing levels of NR2a expression in that group. Cell lines expressing neither NR2 subunit were not responsive to MK801, indicative of its specific targeting of NMDAR.  
 (H) Among the cell lines, DanG expressed the highest level of NR2b and was the most responsive to MK801 treatment in the modified invasion assay. A representative picture from the MK801-treated DanG cells showed markedly decreased numbers of invading cells compared to the control group. Pictures were originally taken in DAPI channel with monochromatic camera, shown with inverted black and white.  
 Data are represented as mean with SEM; a two-tailed Student's t test was performed to compare control and treatment groups from (A)–(E); in (F) and (G); data were normalized to the control group each time, thus a two-tailed one-sample t test was performed to determine if the ratio was significantly different from hypothetical value 1, representing the control. \*p < 0.05, \*\*p < 0.01, \*\*\*p < 0.001.  
 See also Figure S3 and Table S3.



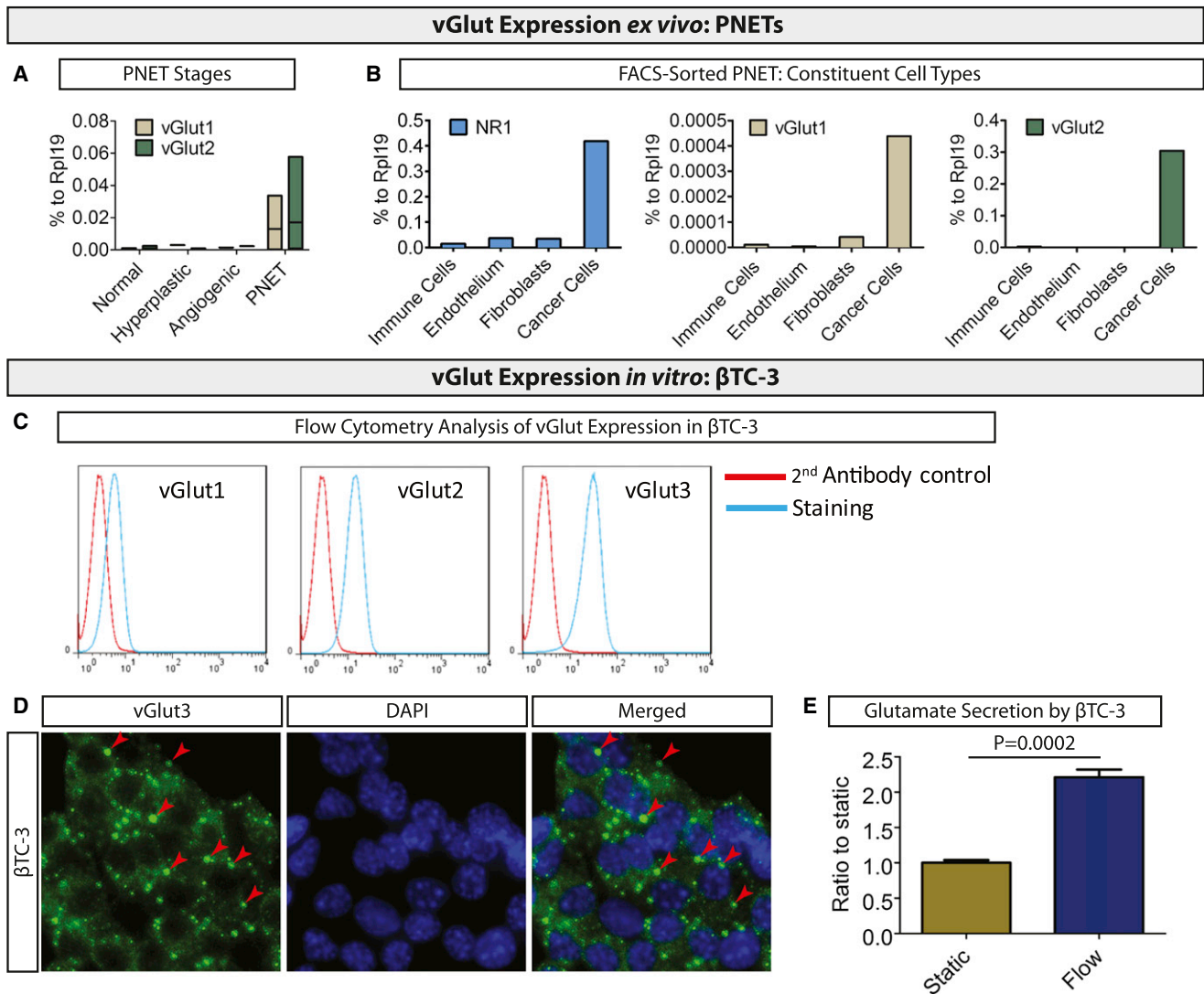


**Figure 4. The NMDAR Circuit in PNET: Upstream Activators**

(A) Comparative analysis of mRNA levels of the glutamate transporters in the different stages in PNET tumorigenesis revealed that expression of both vGlut1 and -2 was increased in PNETs as compared to normal pancreatic islets and premalignant stages. Normal islet: three independent islet pools; hyperplastic and angiogenic islet: one islet pool each; PNETs: 14 tumors. Floating bars showing minimum to maximum with line showing the mean.

(B) Ex vivo, qRT-PCR with cDNA generated from FACS-sorted constituent cell types from PNETs revealed that cancer cells were the major expressers of NR1, vGlut1, and vGlut2, consistent with possible autocrine glutamate to NMDAR signaling. Data shown was from one cell sorting. Sortings were repeated three times, with similar results. Each cell sorting was performed by pooling multiple PNETs from one to two mice. FACS, fluorescence-activated cell sorting.

(C) In vitro, all three vGlut family proteins were expressed in βTC-3 cancer cells generated from a mouse PNET, as shown by flow cytometric analysis with specific antibodies.

(D) Immunocytochemistry confirmed typical punctate cytoplasmic staining of vGlut3 in βTC-3 cells. (Red arrow heads, vGlut3.)

(E) Interstitial flow (Figure 3B) increased glutamate concentration in the medium of the transwell invasion assay as compared to the static condition. Unpaired t test, one-tailed. The data are represented as mean with SEM; the data shown was from one of >5 replicate experiments, each with similar trends. See also Figure S4.

decreased phosphorylation of NR2b and its downstream effectors. Notably, however, MK801-treated cancer cells in the modified invasion assay were still more invasive than cancer cells in the static assay (Figure 3C). It is possible that the CaMK-IV phosphorylation was sufficient to confer the remaining 1.5-fold increase in invasiveness when compared to the static group, whereas the other phosphorylated proteins contributed to the

near-6-fold higher levels of the flow group with no inhibition of NMDAR. Concordantly, the knockdown of CaMK-IV expression with siRNA, which largely abrogated invasiveness with minimal effect on proliferation, supports the selective involvement of this kinase in orchestrating an invasive program (Figure S7). Taken together, we infer that the MEK-MAPK pathway is preferentially governing proliferation and survival

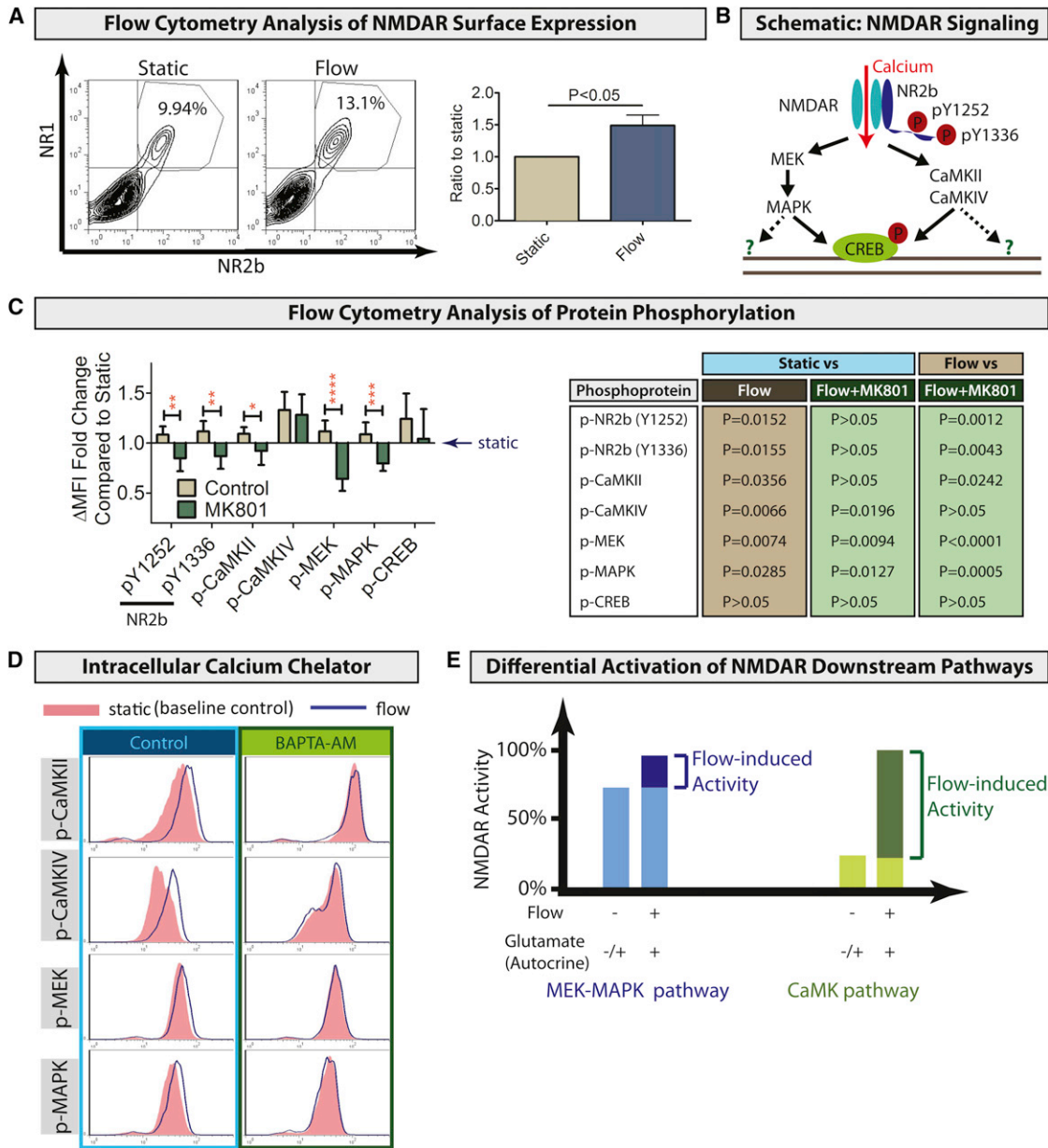


**Figure 5. The NMDAR Circuit in Cancer: Downstream Effectors**

(A) Hydrodynamic pressure and flow through transwells enhanced cell-surface expression of the NMDAR on  $\beta$ TC-3 cells, as revealed by flow cytometry analysis with live cancer cells. Data are represented as mean with SEM.

(B) Schematic of NMDAR signaling: receptor activation leads to calcium-dependent stimulation of two major downstream signaling pathways: the CaMK-II/IV pathway and the MEK-MAPK pathway; NR2b phosphorylation at Y1252 and Y1336 are known to potentiate NMDAR activity. CaMKII, calmodulin kinase type II; CaMKIV, calmodulin kinase type IV; MEK, MAPK/ERK kinase; MAPK, p44/p42 mitogen-activated protein kinase; CREB, cAMP response element-binding protein.

(C) Flow in the modified transwell invasion assay promoted NR2b phosphorylation in  $\beta$ TC-3 cells, and activated both CaMK and MEK-MAPK pathways downstream of NMDAR, which led to CREB phosphorylation. (\* $p < 0.05$ , \*\* $p < 0.01$ , \*\*\* $p < 0.001$ , \*\*\*\* $p < 0.0001$ ) MFI, mean fluorescence intensity;  $\Delta$ MFI, difference of MFI between staining and negative control. One-sample t test was performed to determine if the ratio generated from each experiments was significantly different from 1, representing  $\Delta$ MFI of the static group. Data are represented as mean with SEM.

(D) These flow-mediated effects could be abolished by an intracellular calcium chelator BAPTA-AM; the red shadow (baseline control, static group) and blue line (flow group) almost totally overlapped in the BAPTA-AM-treated group (right), as compared to the separate lines in the control group (left).

(E) A schematic, based on the MFI analysis, suggesting that the MEK-MAPK and CaMK pathways are differentially activated. In static conditions, the MEK-MAPK pathway was already highly activated. In flow conditions, including increased secretion of glutamate, the increased NMDAR phosphorylation only modestly increased MEK-MAPK pathway activity. In contrast, the CaMK pathway activity, which was comparatively low in static condition, is appreciably upregulated by flow conditions.

See also Figure S5.

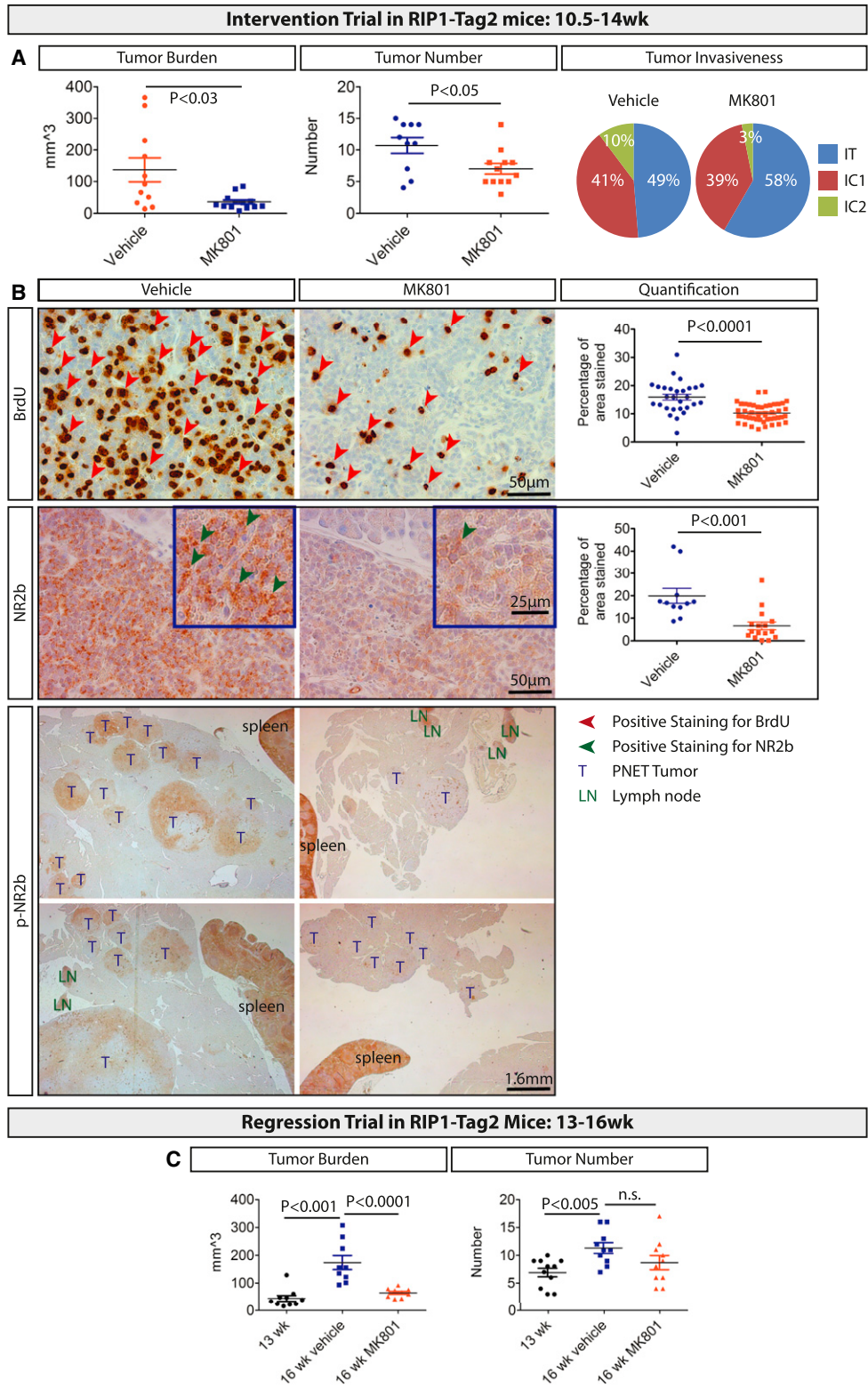


**Figure 6. Functional Importance of NMDAR Signaling in Cancer—In Vivo Evidence**

(A) A preclinical intervention trial targeting early-staged tumors in the RIP1-Tag2 model of PNET using the NMDAR antagonist MK801 decreased tumor burden, tumor number, and the incidence of highly invasive carcinomas in RIP1-Tag2 mice (n = 9–12 mice per group). Definition: IT, tumor margin < 10% invasive; IC1, margin 10%–50% invasive; IC2, margin > 50% invasive. At least 39 tumors per group were graded.

(legend continued on next page)

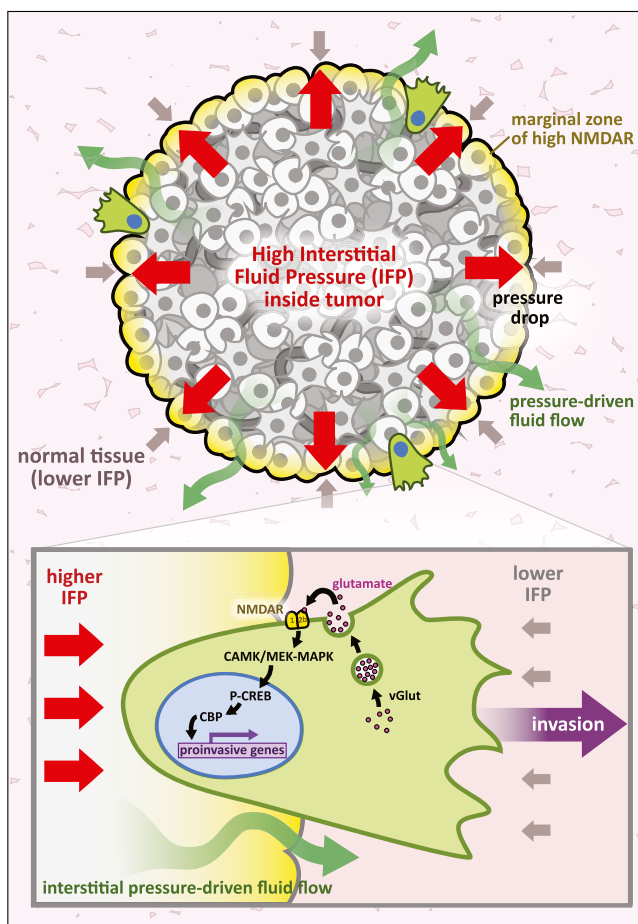


**Figure 7. A Model: Interstitial Flow Activates Glutamate-to-NMDAR Signaling in the Tumor Microenvironment**

At the margins of solid tumors, an interstitial fluid pressure (IFP) drop and consequent fluid flow into adjacent normal tissue induces membrane localization and phosphorylation of the mechanosensitive NMDAR, and elevates expression of glutamate transporters and consequent secretion of glutamate, constituting an autocrine signaling circuit that stimulates cancer cell proliferation (data not shown) and invasiveness. Downstream of glutamate-activated NMDAR, the CaMK-II/IV and MEK-MAPK signal transducers in turn phosphorylate and activate the transcription factor CREB, which associates with the CREB-binding protein (CBP) to regulate a presumptive transcriptional program that mediates tumor growth and invasion. See also [Figure S7](#).

downstream of NMDAR activation, whereas the CaMK pathway, in particular CaMK-IV, is playing the major role in invasion. Still to be clarified in future studies is the role of glutamate-stimulated AMPAR signaling, which is implicated in invasion ([Figure 3C](#)); AMPAR signaling would also be abrogated by BAPTA but not MK801, thus potentially explaining the differences in degrees of inhibition of downstream effector phosphorylation and of invasiveness.

### Therapeutic Benefits of Inhibiting NMDAR Signaling in Tumors

The NMDAR inhibitor MK801 has previously shown antitumoral effects when used to treat various xenograft tumors ([North et al., 2010a](#); [North et al., 2010b](#)). Our study broadens the scope, demonstrating therapeutic efficacy of MK801 in an immunocompetent mouse model of endogenous tumor progression. In addition, whereas tissue invasion cannot be thoroughly assessed in traditional subcutaneous xenografts, this GEMM revealed a role for NMDAR in cancer invasion. Notably, the effect of MK801 in vivo was not as striking as that in vitro, and we suggest an explanation: MK801 has a very short half-life, of about an hour ([Wegener et al., 2011](#)). Therefore, in tumors in vivo the exposure was only for 1 hr a day, whereas in the flow-modified invasion assay, the drug was continuously present. As mentioned previously, we infer that PNET survival and invasion are governed by different downstream pathways. Thus, the 1 hr daily exposure experienced by tumors in vivo might be sufficient to markedly impair proliferation but insufficient to fully inhibit invasion.

Although demonstrably important, NMDAR is not the sole driver of invasion in the RIP1-Tag2 model: various regulatory pathways have been proved instrumental for PNET invasion, including IGF-2/IGF-1R signaling ([Christofori et al., 1994](#); [Lopez and Hanahan, 2002](#)), loss of E-cadherin and altered NCAM function ([Perl et al., 1999](#); [Perl et al., 1998](#)), loss of desmosomal adhesions ([Chun and Hanahan, 2010](#)), and extracellular matrix degrading enzymes supplied by immune cells ([Joyce et al., 2004](#)). Therefore, the incomplete inhibition of PNET tumor invasiveness by NMDAR antagonists may also reflect parallel, independent capabilities manifested by these other signaling events; the possibility that flow-activated glutamate-to-NMDAR signaling regulates one or another of these various proinvasive signaling pathways deserves future investigation.

### Implications of NMDAR Pathway Activation in Human Cancer

Our experimental design, which focused on the mechanism and effects of NMDAR activation in a GEMM of human cancer, involved only a limited (albeit provocative) survey for evidence of NMDAR signaling in different forms of human cancer. There are, therefore, several considerations. First, because NMDAR is in some cases evidently upregulated at the tumor periphery or in tissue-invading cancer cells, TMAs composed of core needle biopsies may miss the informative margins. Moreover, genome-wide expression-profiling data (e.g., from TCGA) may in some cases fail to identify such focal upregulation of mRNA at the margins, obscured by the predominant core of large solid tumors. Second, although we clearly implicated the NR2b subunit in the stimulation of tumor invasion and aggressiveness in the PNET model, we cannot exclude the involvement of alternative NMDAR subunits in other tumor types. In our in vitro survey of human cancer cell lines, some did not express high NR2b, but rather NR2a (such as MDAMB157, SUIT2), and these

(B) MK801 treatment decreased tumor proliferation (BrdU staining), NR2b expression at tumor periphery, and NR2b phosphorylation. BrdU,  $n = 14$ –25 tumors/three mice per group; NR2b,  $n = 11$ –16 tumors/four to five mice per group; p-NR2b,  $n =$  minimum of six mice per group.

(C) Similarly, a regression trial targeting late-stage tumors with MK801 also had antitumoral effects.  $n = 9$ –12 mice per group.

Data are represented as mean with SEM. See also [Figure S6](#).

were also responsive to MK801; in contrast, cell lines expressing neither subunit were poorly responsive to MK801. Finally, the three vGlut transporters may be variably expressed; whereas all were expressed in the PNET model, this might not be the case in other tumor types. Thus the three vGluts as well as the various NMDAR subunits should be audited in the context of surveying human tumor types, ideally incorporating in situ histological methods that can detect localized upregulation at tumor margins and invasive fronts.

### Translational Implications of NMDAR Antagonists for Cancer Therapy

The results collectively suggest that inhibition of NMDAR signaling could have therapeutic benefit in some forms of human cancer. There are, nevertheless, additional considerations. First, patient selection will likely be important. We observed heterogeneous expression of NMDAR in the human cancer TMA survey, as well as varying responses to MK801 treatment in a panel of human cancer cell lines and in a mouse model of breast cancer. Therefore, NMDAR antagonists may be more effective in patients with broader (less focal/peripheral) and higher expression/activation of the NMDAR signaling axis. Additionally, combination therapies with conventional drugs targeting the tumor core along with NMDAR inhibitors targeting the invasive periphery might prove beneficial; moreover, because AMPAR is implicated as a second proinvasive glutamate receptor (Figure 3C), it will be of interest to explore combinatorial targeting of NMDAR and AMPAR.

A second and important consideration is that refined NMDAR inhibitors are needed. As mentioned previously, the short half-life of MK801 may partially account for its incomplete inhibition of tumor invasiveness; as such, a second-generation drug with a longer half-life and better exposure would likely improve efficacy. Additionally, in light of the well-known (side) effects of NMDAR antagonists on learning, memory, and behavior (Wu et al., 2005), it would be highly desirable to develop new NMDAR antagonists that don't cross the blood-brain-barrier. Although such drugs might not have optimal efficacy in glioma, they would likely prove more tolerable clinically for patients with NMDAR-expressing tumors outside of the CNS. Finally, inhibitors of glutamate biosynthesis and secretion are also worth investigating as agents for targeting this proinvasive signaling axis.

### Perspective

In conclusion, this study reveals how cancer cells hijack the glutamate-to-NMDAR signaling pathway operative in neurons to instead promote invasive tumor growth. These findings potentially link the long-recognized existence of high interstitial fluid pressure (IFP) in tumors with the hallmark capability for tumor invasion, whereby comparatively higher IFP in solid tumors creates a pressure drop at the tumor margin, with consequent fluid flow into adjacent normal tissue. Via mechanosensory transduction, this pressure drop and fluid flow evidently activate autocrine glutamate secretion, concomitant with NMDAR phosphorylation and transport to the cell surface to engage the glutamate ligand, with consequent activation of downstream signaling (Figure 7). The results establish a potentially widespread mechanism for inducing tumor invasiveness. This mech-

anism offers a potentially important target for future cancer therapeutics, whereby long-lasting, periphery-acting NMDAR antagonists may have promise for treating certain human cancers.

## EXPERIMENTAL PROCEDURES

### Genetically Engineered Mouse Model of Cancer

The RIP1-Tag2 mice (Hanahan, 1985) were bred and genotyped as previously described (Herzig et al., 2007). In brief, RIP1-Tag2 mice are transgenic mice, inbred into C57Bl/6, carrying a hybrid oncogene composed of the SV40 early region, encoding the large and small T antigen oncoproteins (Tag), fused to rat insulin gene promoter (RIP). Male mice heterozygous for the RIP1-Tag2 transgene are used for breeding with wild-type C57Bl/6J females. Pups were genotyped for SV40 oncogene using qRT-PCR by Transnetyx (Cordova, TN, <http://www.transnetyx.com/>). The qRT-PCR probes are designed by the company and procedures are detailed on the company's website. The probes for conventional genotyping using PCR detection are listed as following: forward primer 5'-GCTCTGCTGACATAGAAGAATGG-3'; reverse primer 5'-GTACTCATTGACTGACTATTCCAG-3' (amplicon 454 bp). Male RIP1-Tag2 mice are typically larger in size than females, therefore, only male mice with body weight over 23 g at starting point of an experiment were included for trials and analysis (See e.g., Chun et al., 2010). The MMTV-PyMT mice were bred and genotyped as previously described (Malanchi et al., 2012). The genetic modifications of the PDAC GEMMs used were listed in the Table S1. The PDAC mice were bred as described previously (Olson et al., 2011).

### Modified Invasion Assay

The hydrostatic-pressure-based modification of the classic Boyden chamber assay was performed as previously described (Shields et al., 2007). In brief, cells were seeded into a mixture of 1.2 mg/ml rat tail collagen type I (BD Biosciences, NJ) and 10%–20% of growth factor reduced matrigel (356231, BD Biosciences, NJ), then placed onto transwell inserts (Millipore <http://www.millipore.com/catalogue/module/C10504>, 12 mm PCF, 8.0  $\mu$ m pore size), and then incubated for one hour at 37°C to solidify the matrix. Additional basal medium was added to the top of the wells to generate ~1cm water head (650  $\mu$ l on the top, 150  $\mu$ l in the bottom for flow condition; 150  $\mu$ l on the top, 650  $\mu$ l on the bottom for the static condition). After overnight incubation, the gels were discarded and the upper side of the membrane was cleaned carefully with cotton tips to ensure that all the cells that didn't cross the membrane were removed. Then, cells on the bottom side of the membrane were fixed with ice-cold methanol and stained with DAPI. Five images/well were taken at constant positions (as illustrated in Figure S3) with a 10 $\times$  objective, which in sum covered most of the area of the membrane. The results were quantified using Fiji Image Analysis software, as described (Schindelin et al., 2012). Each experiment was performed in triplicate and repeated at least three times.

### Analysis of Protein Phosphorylation in the Invasion Assay

The cancer cells were incubated on 6-well hanging inserts (FA-353493, BD Biosciences, NJ) in three different conditions as described in Figure 3B: static, flow and flow plus MK801, following the same gel casting protocol described in Modified Invasion Assay. The gels from the invasion assays mimicking 3D culture were collected from the transwells and digested with collagenase D (11088866001, Roche) according to manufacturer's protocol to release the cells. The cells were counted using a cell counter (Countess Cell Counter, Life Technologies), and equal numbers of cells were distributed into individual wells or tubes for antibody staining. For the intracellular staining, the cells were fixed with Cytofix/Cytoperm buffer (BD Biosciences, NJ), whereas for analysis of NMDAR surface expression, the cells were not fixed. Then the cells were blocked with an anti-mouse CD16/32 Fc blocking agent (BioLegend <http://www.biolegend.com/>). Primary antibodies were diluted 1:100 in the blocking solution, and secondary antibodies (donkey-anti-rabbit IgG Alexa488 A21206, donkey-anti-rabbit IgG Alexa568 A10042, goat-anti-mouse IgG Alexa488 A11029, donkey-anti-mouse Alexa647 A31571, all from Life Technologies) were diluted at 1:1000 in the staining solution (BD Biosciences, NJ). Staining was performed on ice for ~30 min. Samples were then subjected

to flow cytometry in a CyAn ADPS flow cytometry analyzer (Beckman Coulter) in the EPFL flow cytometry core facility. Flow cytometry data were analyzed with FlowJo software, and mean fluorescence intensity (MFI) was calculated using geometric mean.

## SUPPLEMENTAL INFORMATION

Supplemental Information includes Extended Experimental Procedures, seven figures, and four tables and can be found with this article online at <http://dx.doi.org/10.1016/j.cell.2013.02.051>.

## ACKNOWLEDGMENTS

We wish to thank M. Luisa Iruela-Arispe, Igor Allaman, and Anita Wolfer for advice, discussions, and insightful comments on the manuscript; Jessica Sordet-Dessimoz and Alessandra Piersigilli for pathology, Jacques Rougemont and Marion Leleu for statistical consultations; Ehud Drori, Mei-Wen Peng, and Jean-Paul Abbühl for help with animal experiments; Yunyun Han, Hsin-Ying Huang, Sukhvinder Sidhu, and all Hanahan lab members for biological samples and discussions; Melody Swartz, Adrian C. Shieh, and Jacqueline Shields for advice and instruction on the modified invasion assay; Janet Iwasa for the schematic figure; and the EPFL School of Life Sciences technology cores and animal care facility. This research was supported by a core grant from EPFL. Some results are based on data generated by the TCGA pilot project.

Received: September 26, 2012

Revised: January 8, 2013

Accepted: February 21, 2013

Published: March 28, 2013

## REFERENCES

- Bai, L., Zhang, X., and Ghishan, F.K. (2003). Characterization of vesicular glutamate transporter in pancreatic alpha- and beta-cells and its regulation by glucose. *Am. J. Physiol. Gastrointest. Liver Physiol.* *284*, G808–G814.
- Bergers, G., Javaherian, K., Lo, K.M., Folkman, J., and Hanahan, D. (1999). Effects of angiogenesis inhibitors on multistage carcinogenesis in mice. *Science* *284*, 808–812.
- Braithwaite, S.P., Adkisson, M., Leung, J., Nava, A., Masterson, B., Urfer, R., Oksenberg, D., and Nikolich, K. (2006). Regulation of NMDA receptor trafficking and function by striatal-enriched tyrosine phosphatase (STEP). *Eur. J. Neurosci.* *23*, 2847–2856.
- Christofori, G., Naik, P., and Hanahan, D. (1994). A second signal supplied by insulin-like growth factor II in oncogene-induced tumorigenesis. *Nature* *369*, 414–418.
- Chun, M.G., and Hanahan, D. (2010). Genetic deletion of the desmosomal component desmoplakin promotes tumor microinvasion in a mouse model of pancreatic neuroendocrine carcinogenesis. *PLoS Genet.* *6*, e1001120.
- Chun, M.G., Mao, J.H., Chiu, C.W., Balmain, A., and Hanahan, D. (2010). Polymorphic genetic control of tumor invasion in a mouse model of pancreatic neuroendocrine carcinogenesis. *Proc. Natl. Acad. Sci. USA* *107*, 17268–17273.
- Dafni, H., Israely, T., Bhujwalla, Z.M., Benjamin, L.E., and Neeman, M. (2002). Overexpression of vascular endothelial growth factor 165 drives peritumor interstitial convection and induces lymphatic drain: magnetic resonance imaging, confocal microscopy, and histological tracking of triple-labeled albumin. *Cancer Res.* *62*, 6731–6739.
- Du, Y.C., Lewis, B.C., Hanahan, D., and Varmus, H. (2007). Assessing tumor progression factors by somatic gene transfer into a mouse model: Bcl-xL promotes islet tumor cell invasion. *PLoS Biol.* *5*, e276.
- DuFort, C.C., Paszek, M.J., and Weaver, V.M. (2011). Balancing forces: architectural control of mechanotransduction. *Nat. Rev. Mol. Cell Biol.* *12*, 308–319.
- Efrat, S., Linde, S., Kofod, H., Spector, D., Delannoy, M., Grant, S., Hanahan, D., and Baekkeskov, S. (1988). Beta-cell lines derived from transgenic mice expressing a hybrid insulin gene-oncogene. *Proc. Natl. Acad. Sci. USA* *85*, 9037–9041.
- Fantozzi, A., and Christofori, G. (2006). Mouse models of breast cancer metastasis. *Breast Cancer Res.* *8*, 212.
- Grippo, P.J., and Tuveson, D.A. (2010). Deploying mouse models of pancreatic cancer for chemoprevention studies. *Cancer Prev. Res. (Phila.)* *3*, 1382–1387.
- Gutmann, R., Leunig, M., Feyh, J., Goetz, A.E., Messmer, K., Kastenbauer, E., and Jain, R.K. (1992). Interstitial hypertension in head and neck tumors in patients: correlation with tumor size. *Cancer Res.* *52*, 1993–1995.
- Hanahan, D. (1985). Heritable formation of pancreatic beta-cell tumours in transgenic mice expressing recombinant insulin/simian virus 40 oncogenes. *Nature* *315*, 115–122.
- Hanahan, D., and Coussens, L.M. (2012). Accessories to the crime: functions of cells recruited to the tumor microenvironment. *Cancer Cell* *21*, 309–322.
- Hanahan, D., and Weinberg, R.A. (2011). Hallmarks of cancer: the next generation. *Cell* *144*, 646–674.
- Hardingham, G.E., and Bading, H. (2010). Synaptic versus extrasynaptic NMDA receptor signalling: implications for neurodegenerative disorders. *Nat. Rev. Neurosci.* *11*, 682–696.
- Harrell, M.I., Iritani, B.M., and Ruddell, A. (2007). Tumor-induced sentinel lymph node lymphangiogenesis and increased lymph flow precede melanoma metastasis. *Am. J. Pathol.* *170*, 774–786.
- Heldin, C.H., Rubin, K., Pietras, K., and Ostman, A. (2004). High interstitial fluid pressure - an obstacle in cancer therapy. *Nat. Rev. Cancer* *4*, 806–813.
- Herner, A., Sauliunaite, D., Michalski, C.W., Erkan, M., De Oliveira, T., Abiatar, I., Kong, B., Esposito, I., Friess, H., and Kleeff, J. (2011). Glutamate increases pancreatic cancer cell invasion and migration via AMPA receptor activation and Kras-MAPK signaling. *Int. J. Cancer* *129*, 2349–2359.
- Herzig, M., Savarese, F., Novatchkova, M., Semb, H., and Christofori, G. (2007). Tumor progression induced by the loss of E-cadherin independent of beta-catenin/Tcf-mediated Wnt signaling. *Oncogene* *26*, 2290–2298.
- Joyce, J.A., Baruch, A., Chehade, K., Meyer-Morse, N., Giraudo, E., Tsai, F.Y., Greenbaum, D.C., Hager, J.H., Bogyo, M., and Hanahan, D. (2004). Cathepsin cysteine proteases are effectors of invasive growth and angiogenesis during multistage tumorigenesis. *Cancer Cell* *5*, 443–453.
- Lau, C.G., and Zukin, R.S. (2007). NMDA receptor trafficking in synaptic plasticity and neuropsychiatric disorders. *Nat. Rev. Neurosci.* *8*, 413–426.
- Lopez, T., and Hanahan, D. (2002). Elevated levels of IGF-1 receptor convey invasive and metastatic capability in a mouse model of pancreatic islet tumorigenesis. *Cancer Cell* *1*, 339–353.
- Malanchi, I., Santamaria-Martínez, A., Susanto, E., Peng, H., Lehr, H.A., Delaloye, J.F., and Huelsken, J. (2012). Interactions between cancer stem cells and their niche govern metastatic colonization. *Nature* *481*, 85–89.
- Marsden, K.C., Beattie, J.B., Friedenthal, J., and Carroll, R.C. (2007). NMDA receptor activation potentiates inhibitory transmission through GABA receptor-associated protein-dependent exocytosis of GABA(A) receptors. *J. Neurosci.* *27*, 14326–14337.
- Nguyen, D.X., Bos, P.D., and Massagué, J. (2009). Metastasis: from dissemination to organ-specific colonization. *Nat. Rev. Cancer* *9*, 274–284.
- Nicoletti, F., Arcella, A., Iacovelli, L., Battaglia, G., Giangaspero, F., and Melchiorri, D. (2007). Metabotropic glutamate receptors: new targets for the control of tumor growth? *Trends Pharmacol. Sci.* *28*, 206–213.
- North, W.G., Gao, G., Jensen, A., Memoli, V.A., and Du, J. (2010a). NMDA receptors are expressed by small-cell lung cancer and are potential targets for effective treatment. *Clin Pharmacol* *2*, 31–40.
- North, W.G., Gao, G., Memoli, V.A., Pang, R.H., and Lynch, L. (2010b). Breast cancer expresses functional NMDA receptors. *Breast Cancer Res. Treat.* *122*, 307–314.
- Olson, P., Chu, G.C., Perry, S.R., Nolan-Stevaux, O., and Hanahan, D. (2011). Imaging guided trials of the angiogenesis inhibitor sunitinib in mouse models predict efficacy in pancreatic neuroendocrine but not ductal carcinoma. *Proc. Natl. Acad. Sci. USA* *108*, E1275–E1284.

- Perl, A.K., Wilgenbus, P., Dahl, U., Semb, H., and Christofori, G. (1998). A causal role for E-cadherin in the transition from adenoma to carcinoma. *Nature* 392, 190–193.
- Perl, A.K., Dahl, U., Wilgenbus, P., Cremer, H., Semb, H., and Christofori, G. (1999). Reduced expression of neural cell adhesion molecule induces metastatic dissemination of pancreatic beta tumor cells. *Nat. Med.* 5, 286–291.
- Poitout, V., Stout, L.E., Armstrong, M.B., Walseth, T.F., Sorenson, R.L., and Robertson, R.P. (1995). Morphological and functional characterization of beta TC-6 cells—an insulin-secreting cell line derived from transgenic mice. *Diabetes* 44, 306–313.
- Prickett, T.D., and Samuels, Y. (2012). Molecular pathways: dysregulated glutamatergic signaling pathways in cancer. *Clin. Cancer Res.* 18, 4240–4246.
- Rzeski, W., Turski, L., and Ikonomidou, C. (2001). Glutamate antagonists limit tumor growth. *Proc. Natl. Acad. Sci. USA* 98, 6372–6377.
- Schindelin, J., Arganda-Carreras, I., Frise, E., Kaynig, V., Longair, M., Pietzsch, T., Preibisch, S., Rueden, C., Saalfeld, S., Schmid, B., et al. (2012). Fiji: an open-source platform for biological-image analysis. *Nat. Methods* 9, 676–682.
- Seidlitz, E.P., Sharma, M.K., Saikali, Z., Ghert, M., and Singh, G. (2009). Cancer cell lines release glutamate into the extracellular environment. *Clin. Exp. Metastasis* 26, 781–787.
- Sharma, M.K., Seidlitz, E.P., and Singh, G. (2010). Cancer cells release glutamate via the cystine/glutamate antiporter. *Biochem. Biophys. Res. Commun.* 391, 91–95.
- Shieh, A.C., and Swartz, M.A. (2011). Regulation of tumor invasion by interstitial fluid flow. *Phys. Biol.* 8, 015012.
- Shields, J.D., Fleury, M.E., Yong, C., Tomei, A.A., Randolph, G.J., and Swartz, M.A. (2007). Autologous chemotaxis as a mechanism of tumor cell homing to lymphatics via interstitial flow and autocrine CCR7 signaling. *Cancer Cell* 11, 526–538.
- Stepulak, A., Luksch, H., Gebhardt, C., Uckermann, O., Marzahn, J., Sifringer, M., Rzeski, W., Stauffer, C., Brocke, K.S., Turski, L., and Ikonomidou, C. (2009). Expression of glutamate receptor subunits in human cancers. *Histochem. Cell Biol.* 132, 435–445.
- Takano, T., Lin, J.H., Arcuino, G., Gao, Q., Yang, J., and Nedergaard, M. (2001). Glutamate release promotes growth of malignant gliomas. *Nat. Med.* 7, 1010–1015.
- Takasu, M.A., Dalva, M.B., Zigmond, R.E., and Greenberg, M.E. (2002). Modulation of NMDA receptor-dependent calcium influx and gene expression through EphB receptors. *Science* 295, 491–495.
- Wegener, N., Nagel, J., Gross, R., Chambon, C., Greco, S., Pietraszek, M., Gravius, A., and Danysz, W. (2011). Evaluation of brain pharmacokinetics of (+)MK-801 in relation to behaviour. *Neurosci. Lett.* 503, 68–72.
- Wu, J., Zou, H., Strong, J.A., Yu, J., Zhou, X., Xie, Q., Zhao, G., Jin, M., and Yu, L. (2005). Bimodal effects of MK-801 on locomotion and stereotypy in C57BL/6 mice. *Psychopharmacology (Berl.)* 177, 256–263.

## EXTENDED EXPERIMENTAL PROCEDURES

### Ethics Statement

All mice used in this study were maintained in a pathogen-free barrier animal facility of the Swiss Federal Institute of Technology Lausanne (EPFL) in accord with Swiss regulations for the care and use of mice in experimental research.

### Immunocytochemistry on Cultured Cells and Immunohistochemistry on Tissue Sections

For immunocytochemistry (ICC), cells were cultured on matrigel-coated slide chambers and fixed with methanol. For immunohistochemistry (IHC) on tissue sections, anaesthetized mice were cardiac-perfused with zinc-formalin and PBS. Harvested tissues were fixed in zinc-formalin overnight and then embedded in paraffin. Antigen retrieval was performed in a citrate buffer (pH = 6.0) in a water bath at 95°C for 20 min. Primary antibodies were incubated at 4°C overnight, and biotinylated secondary antibodies (donkey anti-rabbit IgG 711-065-152 and donkey anti-mouse IgG 715-065-150, both from Jackson Immunologicals Research) were incubated at room temperature for 30 min, followed by incubation with avidin/biotinylated enzyme complex (Vectastain Elite ABC kit [Vector Labs <http://www.vectorlabs.com/>]) for 30 min at room temperature, and finally were visualized with the peroxidase substrate DAB (Sigma-Aldrich, D5637-1G) for 8 min at room temperature. Finally, the stained tissue sections were counterstained with Meyer's hematoxylin.

### Semiquantification of NR2b Staining in Mouse PNET

The pictures were taken with 40× objectives, and NR2b staining was semiquantified with Fiji Image Analysis Software (Schindelin et al., 2012) using similar methodology to that described previously (Prykhozhij, 2010). In brief, the images were split into three channels (red, green, and blue) by the Fiji software. In our experiments, the red channel corresponded to the Meyer's hematoxylin staining of the cells, whereas the blue channel corresponded to the NR2b (DAB) staining. Therefore, the red channel was used to measure the total tumor area, whereas the blue channel was used to measure the DAB-stained area. By comparing these two values, one can measure the percentage of DAB (NR2b) staining to all (tumor) area. Stronger DAB staining results in higher signal in the blue channel, thus the increased percentage to all area. This percentage thus represents a measure of both staining intensity and stain area, instead of the percentage of positively stained cells only.

### Antibodies

NR1, antibody: Thermo Scientific (PA3-102) for both IHC and flow cytometry. NR2b: Neuromab (clone N59/36) for ICC and flow cytometry; Thermo Scientific (PA3-105) for IHC. Phospho-NR2b (pY1252 and pY1336) antibodies: Life Technologies (485200 and 485300, respectively) for both IHC and flow cytometry. vGlut antibodies: Neuromab (Clone: N28/9 for vGlut1; N29/29 for vGlut2; N34/34 for vGlut3). Phospho-CaMKIV antibody: Abcam (ab59424). Phospho-CaMKII: Cell Signaling (3361). Phospho-MEK1/1: Cell Signaling (9154). Phospho-p44/42 MAPK: Cell Signaling (9101). Phospho-CREB: Cell Signaling (9191). Antibodies used for FACS sorting were all fluorophore-conjugated antibodies: APC/Cy7-CD45 (BioLegend 103116), APC-CD45 (eBioscience 17-0454-82), FITC-CD31 (BioLegend 102506), APC-CD140a (eBioscience 17-1401), PE-CD140a (eBioscience 12-1401-81), PE-CD11b (eBioscience 12-0112-85), FITC-Gr1 (553127, BD Biosciences, NJ). The antibodies were used at 1:100 dilution for flow cytometry experiments, and at 1:500 for ICC and IHC.

### Chemicals

MK801 and GYKI52466 were purchased from Sigma-Aldrich and Tocris (<http://www.tocris.com/>), respectively, and both were used at 100 μM for in vitro experiments. Memantine was purchased from Tocris. BAPTA-AM was purchased from Enzo (<http://www.enzolfsciences.com/>).

### Proliferation/Apoptosis Assay

Proliferation assays were performed in vitro using a BrdU staining kit (BD Biosciences, NJ). BrdU was added to the culture medium and incubated for 2 hr at 37°C. Apoptosis assays were performed in vitro using a PI/AnnexinV kit (BD Biosciences, NJ). Cells were washed twice with PBS (Life Technologies) and trypsinized using TryPLE Express (Life Technologies). The stainings were performed as described in the protocols in the kits, and the cells were analyzed by flow cytometry. For the screening of MK801 effects on various human cancer cell lines, cell viability analyses were performed with the CellTiter-Glo Luminescent Cell Viability Assay (Promega <http://www.promega.com/>) following manufacturer's protocol. In brief, 1,250–5,000 cells were seeded per well in 96-well plates on day 0, and the next morning the medium was changed to either complete medium (control group) or complete medium with 100 μM MK801 (MK801 treatment group). The analysis was performed on day 3. Experiments were performed in quadruplicates and repeated at least four times.

### siRNA Transfection

Pre-designed siRNAs by the manufacturer (FlexiTube siRNA service, Qiagen, <http://www.qiagen.com/>) were transfected using Lipofectamine 2000 (Life Technologies) according to the protocol from the manufacturer. Assays were performed 48–72 hr posttransfection.



### Fluorescence-Activated Cell Sorting of PNETs

Cancer cells were collected from tumors excised from 14- to 17-week-old mice. The samples were prepared as described previously (Song et al., 2005). Tumors were carefully separated from adjacent acinar cells, and digested with collagenase II (17101015, Life Technologies), collagenase IV (17104019, Life Technologies) and DNase (18047019, Life Technologies) to release individual cancer cells. Surface markers were used to separate PNETs into several different compartments: infiltrating immune (inflammatory) cells (CD45+) or nonimmune cells (CD45-), further subdivided by other cell-surface markers, for  $\beta$  tumor cells (CD45-, CD140a-, CD31-), endothelial cells (CD45-, CD140a-, CD31+) and fibroblasts (CD45-, CD140a+).

### mRNA Reverse Transcription and Quantitative Real-Time PCR

mRNA extractions from cultured cell lines were performed with the Qiagen RNeasy kit (74106), and extractions from FACS-sorted PNETs with the Qiagen miRNeasy kit (217004). Reverse transcription into cDNA was performed with Superscript II (Life Technologies). qRT-PCR was performed with vendor-designed Taqman probes purchased from Applied Biosystems (See Table S4), using the Rotor-Gene Q system (Qiagen). For assessing FACS sorted samples, mRNA was generated from sorted cells derived by pooling all excisable solid tumors from one or two mice. All qRT-PCR reactions were performed as duplicates or triplicates. Results were normalized to the housekeeping genes *rpl19* (for mouse) and *rpl14* (for human).

### Measurement of Glutamate Concentration

Glutamate levels were measured with the Amplex Red glutamine acid/glutamate oxidase assay kit (Life Technologies), following protocols described in the manual.

### BAPTA-AM Treatment

BAPTA-AM (Enzo) was diluted in DMEM medium to 3  $\mu$ M and applied to the cells. After a 30 min incubation at 37°C, the cells were washed twice with PBS and then incubated for another 30 min at 37°C in complete DMEM. The cells were then used for experimental analysis.

### Gene Expression Analysis in the Different Stages of Tumorigenesis

mRNA from normal, hyperplastic and angiogenic islets, and solid tumors was collected and generated by Hanahan lab staff at UCSF as described previously (Chun et al., 2010; Olson et al., 2009). Reverse transcription into cDNA and real-time PCR was performed as described in mRNA Reverse Transcription And Quantitative Real-Time PCR.

### Preclinical Trials with MK801 in RIP1-Tag2 Mice

Intervention trials ran for 3.5 weeks, from 10.5–14 weeks of age in the highly synchronous RIP1-Tag2 mouse model of tumorigenesis, whereas regression trials involved treating tumor-bearing mice from 13–16 weeks of age. MK801 was diluted in normal saline and given intraperitoneally at 1 mg/kg daily, 5 days a week. Memantine was also diluted in normal saline, and given at 10 mg/kg following the same protocol. Cohorts were matched by age and weight (littermates were used if available), and were given weight-matched amount of normal saline; only male mice were used in light of body weight and tumor volume differences between males and females.

### Preclinical Trials with MK801 in Orthotopic Transplantation Model of MMTV-PyMT Breast Cancer

The detailed protocol was described previously (Malanchi et al., 2012). Harvested breast cancer cells from a mammary tumor in a female MMTV-PyMT mouse were cultured on collagen-coated plates overnight (with or without 100  $\mu$ M MK801). The next day, equal numbers of cells from either control or MK801-treated groups were orthotopically injected (immersed in matrigel) into a single mammary fat pad (either the ninth [right abdominal], or both the ninth [right] and the fourth [left abdominal]) in cohorts of nine wide-type FBVN females. Treatment with MK801 started 2 days after the transplantation, following the same dosing regimen as detailed in Preclinical Trials with MK801 in RIP1-Tag2 Mice. Mice were sacrificed after 3 weeks of treatment, and tumor burden was assessed by weight (g) of excised tumors.

### Tissue Microarrays

Tissue microarrays were purchased from US Biomax (<http://www.biomax.us/>) (Pancreatic cancer: PA481. Ovarian cancer: OV241a. Breast cancer: BCA961. Glioma: GL241a. Prostate cancer: PR481). The staining was performed as described in Immunocytochemistry on Cultured Cells and Immunohistochemistry on Tissue Sections. For the analysis of the breast cancer TMA, we categorized the samples into 4 levels of NR2b expression according to the NR2b IHC staining intensity. In the meantime, according to the data listed on manufacturer's website (<http://www.biomax.us/tissue-arrays/Breast/BRC961>), we categorized the samples into 3 clinical subtypes: luminal, basal and HER2. Samples with HER2 expression +++ or ++/+++ were defined as belonging to the HER2 group; the remaining samples were defined as luminal subtype if ER and or PR staining was positive, and the basal subtype was defined as ER and PR negative. Out of the 11 samples defined as basal subtype, two samples from one patient showed ER negativity but low positivity for PR staining and was assumed to be false positive.

### Statistic Analysis

Statistics were performed with Prism 5 (GraphPad Software) and Excel. Unless stated otherwise, the Student's t test was used for nonpaired experiments, and the paired Student's t test was used for paired experiments. For paired experiments that did not follow a Gaussian distribution, the two-tailed Wilcoxon matched pairs test was performed, and a test for effective pairing was also performed and quantified by calculating the nonparametric Spearman correlation coefficient (rs). For paired experiments that were each time normalized to a control sample, a ratio was obtained. The ratios from repeated experiments were then analyzed with the one-sample t test to determine if the ratio was different from 1 (control).

In the preclinical trials, Grubbs' outlier test (also known as the ESD [extreme studentized deviate] method) was performed for data pertaining to tumor burden or tumor number, using online software from GraphPad website (<http://graphpad.com/quickcalcs/Grubbs1.cfm>). Samples with  $p < 0.05$  was considered as outliers of that experiment. A maximum of one outlier per group was eliminated. The Mann-Whitney test was used for assessing the differences in tumor burden and tumor number. A  $p$  value  $< 0.05$  was considered significant. Error bars shown in figures represent standard error of the mean (SEM).

### Clinical Data Analysis

Detailed patient data were obtained from the TCGA (The Cancer Genome Atlas) website through the controlled access data tier. This access was authorized by the NIH. The publically available gene expression data were downloaded from the TCGA data portal, in which the AgilentG4502A\_07 Z score was used to assess gene expression levels; the Z score of each sample represents the number of standard deviations away from the mean of the whole analyzed data set. The patients' clinical data and their corresponding gene expression data were matched manually, and only patients with both valid clinical and gene expression data were included in the analysis. By setting  $z = 0$  as a cut off value, we divided patients into NR2b (*grin2b*) low (Z score  $< 0$ ) and NR2b high (Z score  $> 0$ ) groups. For vGlut gene expression analysis, we divided the three vGlut genes (*slc17a6*, *slc17a7*, *slc17a8*) into low and high expressers, again by using  $z = 0$  as cut-off within both NR2b low and high groups. The survival analysis was done using the Log-rank (Mantel-Cox) test and presented as Kaplan-Meier curves (Figures 2D, 2F, and S2). For combined analysis of NR2b and vGlut family genes, the Logrank test for trend was performed to determine if there was a trend in the four groups. The NR2b/vGlut low and NR2b/vGlut high groups were isolated, and the Logrank test was performed again to compare only the two groups.  $p < 0.05$  was considered significant.

### SUPPLEMENTAL REFERENCES

- Collisson, E.A., Sadanandam, A., Olson, P., Gibb, W.J., Truitt, M., Gu, S., Cooc, J., Weinkle, J., Kim, G.E., Jakkula, L., et al. (2011). Subtypes of pancreatic ductal adenocarcinoma and their differing responses to therapy. *Nat. Med.* 17, 500–503.
- Harvey, J.M., Clark, G.M., Osborne, C.K., and Allred, D.C. (1999). Estrogen receptor status by immunohistochemistry is superior to the ligand-binding assay for predicting response to adjuvant endocrine therapy in breast cancer. *J. Clin. Oncol.* 17, 1474–1481.
- Heiser, L.M., Sadanandam, A., Kuo, W.L., Benz, S.C., Goldstein, T.C., Ng, S., Gibb, W.J., Wang, N.J., Ziyad, S., Tong, F., et al. (2012). Subtype and pathway specific responses to anticancer compounds in breast cancer. *Proc. Natl. Acad. Sci. USA* 109, 2724–2729.
- Olson, P., Lu, J., Zhang, H., Shai, A., Chun, M.G., Wang, Y., Libutti, S.K., Nakakura, E.K., Golub, T.R., and Hanahan, D. (2009). MicroRNA dynamics in the stages of tumorigenesis correlate with hallmark capabilities of cancer. *Genes Dev.* 23, 2152–2165.
- Onitilo, A.A., Engel, J.M., Greenlee, R.T., and Mukesh, B.N. (2009). Breast cancer subtypes based on ER/PR and Her2 expression: comparison of clinicopathologic features and survival. *Clin. Med. Res.* 7, 4–13.
- Prykhodzij, S.V. (2010). In the absence of Sonic hedgehog, p53 induces apoptosis and inhibits retinal cell proliferation, cell-cycle exit and differentiation in zebrafish. *PLoS ONE* 5, e13549.
- Song, S., Ewald, A.J., Stallcup, W., Werb, Z., and Bergers, G. (2005). PDGFRbeta+ perivascular progenitor cells in tumours regulate pericyte differentiation and vascular survival. *Nat. Cell Biol.* 7, 870–879.
- van Agthoven, T., Timmermans, M., Foekens, J.A., Dorssers, L.C., and Henzen-Logmans, S.C. (1994). Differential expression of estrogen, progesterone, and epidermal growth factor receptors in normal, benign, and malignant human breast tissues using dual staining immunohistochemistry. *Am. J. Pathol.* 144, 1238–1246.
- Wen, P.Y., and Kesari, S. (2008). Malignant gliomas in adults. *N. Engl. J. Med.* 359, 492–507.

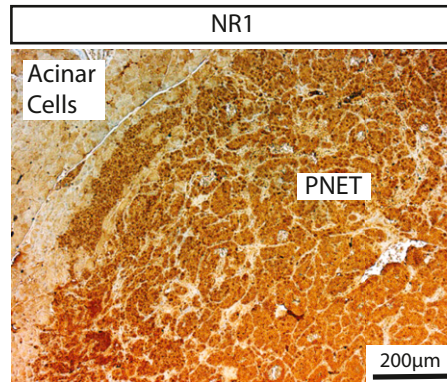


**Figure S1. NR1 Is Also Expressed in PNETs, Related to Figure 1**

Immunohistochemistry revealed that the NMDAR subunit 1 (NR1) was expressed by the PNETs in the RIP1-Tag2 mouse model. More than ten tumors from five mice were analyzed, and the picture shown is representative.

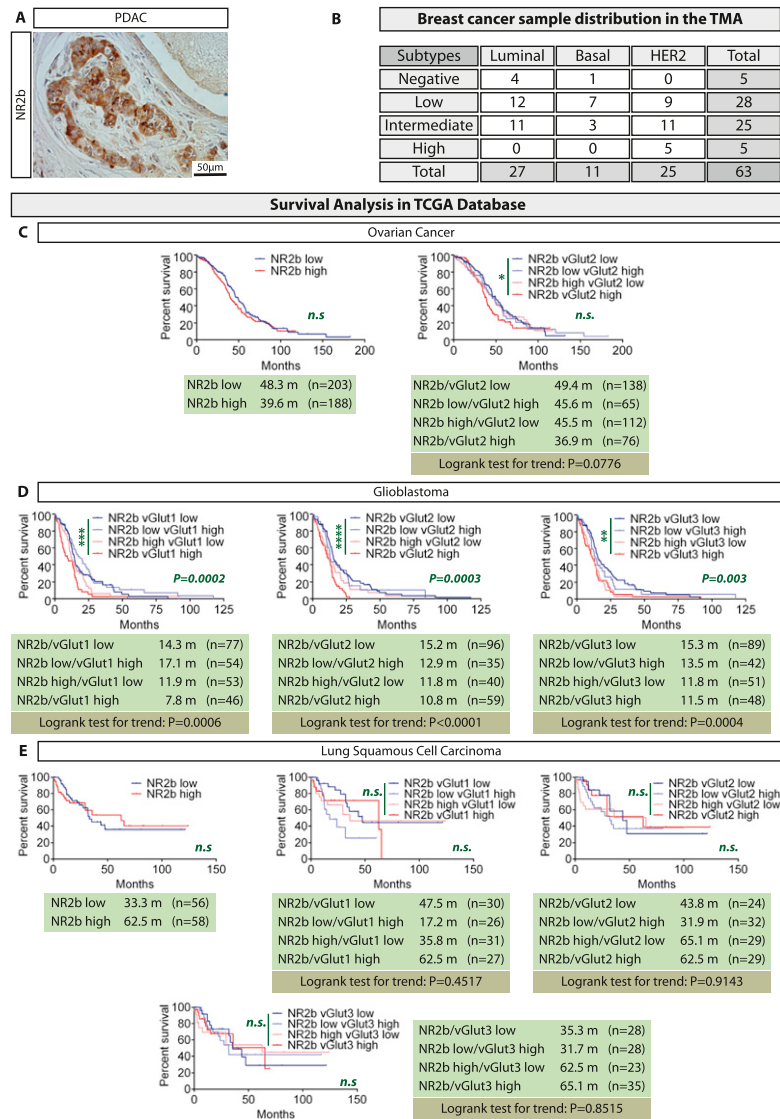


**Figure S2. Involvement of NMDAR Signaling in Human Cancers—Descriptive Evidence, Related to Figure 2**

(A) In a limited survey of human pancreatic adenocarcinoma TMA, high expression of NR2b was identified in a subset of cancer cells. One representative image is shown.

(B) The NR2b was differentially expressed in different breast cancer subtypes. The subtypes were defined as described in the [Extended Experimental Procedures](#). The contingency table was analyzed with Chi-square test, with Chi-square = 13.08, degree of freedom = 6, and  $p = 0.0418$ . A total of 72 breast cancer samples from 36 patients in the TMA were analyzed. Two sarcoma samples were excluded, as were seven other cancer samples due to poor sample quality, tissue detachment from the slides, etc. Thus NR2b expression was assessed in 63 breast cancer samples.

(C) NMDAR signaling is implicated in ovarian cancer, as high expression of vGlut2 and NR2b was a signature for poor prognosis in advanced stage ovarian cancer patients. The prognosis difference was not significant when patients from all different stages were pooled. However, when only stage III patients were included, who represented the majority of patients in the TCGA data sets (391 stage III patients out of 503 total patients with documented survival data) the survival difference was significant with median overall survival increasing from 36.9 months in NR2b/vGlut2 high patients to 49.4 months in NR2b/vGlut2 low patients.

(D) High expression of NR2b alone was a signature for poor prognosis in glioblastoma (GBM) patients. Subdividing patients into vGlut high/low groups in both NR2b low and high group further separated the survival curves. Because GBM is twice as common in white people compared to black people and is 40% more prevalent in males than in females ([Wen and Kesari, 2008](#)), we selected white, male patients for survival analysis.

(E) Similar analysis was performed in the TCGA squamous cell lung carcinoma data set, and NMDAR signaling axis didn't show prognostic significance in this data set.

n.s., not significant. \* $p < 0.05$ , \*\* $p < 0.01$ , \*\*\* $p < 0.001$ , \*\*\*\* $p < 0.0001$ . Log rank test was performed for the survival analysis, and P values were shown on the Kaplan-Meier curves. For data with more than two curves, i.e., combined analysis of NR2b and vGlut family genes, log rank test for trend was performed to assess if there was a survival trend in the four curves analyzed. In addition, in the combined analysis of NR2b and vGlut family genes, two curves presumably representing low and high NMDAR signaling axis, i.e., the NR2b-low/vGlut-low versus the NR2b-high/vGlut-high groups, were isolated for another log rank test to compare these two groups. Also see [Table S2](#).

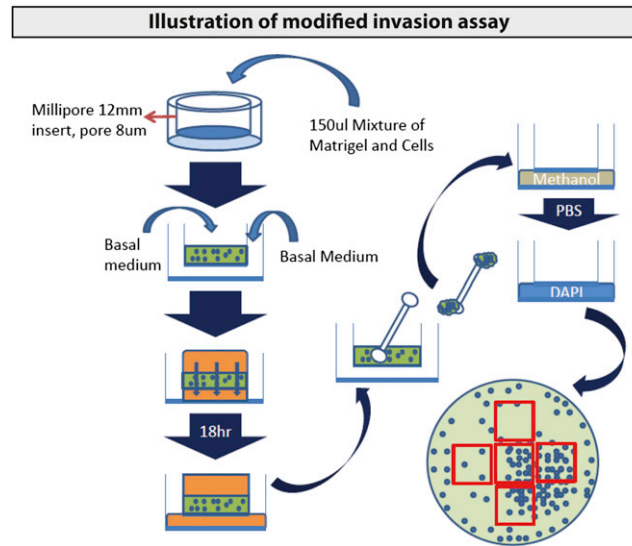


**Figure S3. Detailed Schematic of the Invasion Assay Mimicking Interstitial Pressure-Driven Flow Conditions, Related to Figure 3**

In the traditional transwell invasion assay, cells are seeded onto a layer of matrigel above a porous disc. The system is static, with no fluid flow. In the modified invasion assay developed in the laboratory of Melody Swartz at EPFL (Shields et al., 2007), cells are seeded onto the porous disc immersed in a matrigel/collagen gel mixture as a 3D culture, and then medium is placed on top of the gel, creating a hydrostatic pressure gradient that generates fluid flow down through the gel/cell mixture and the porous disc into the lower chamber.

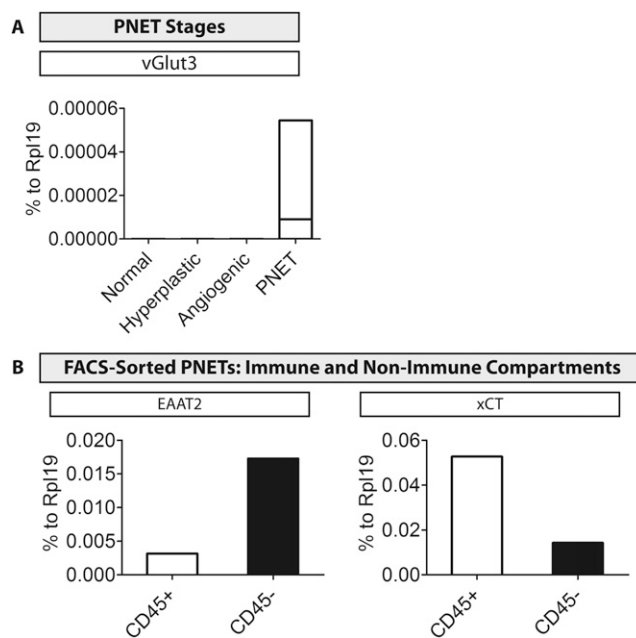


**Figure S4. Additional Evaluation of Glutamate Transporter Expression in PNET, Related to Figure 4**

(A) Comparative analysis of mRNA levels of the glutamate transporters in the different stages in PNET tumorigenesis revealed that expression of vGlut3 was increased in PNETs as compared to normal pancreatic islets and premalignant stages. Normal islet: three independent islet pools; hyperplastic and angiogenic islet: one islet pool each; PNETs: 14 tumors. Floating bars showing minimum to maximum, and line showing mean.

(B) Ex vivo, qRT-PCR with cDNA generated from FACS-sorted constituent cell types from PNETs revealed that CD45<sup>-</sup>, nonimmune cells (with the vast majority being cancer cells) were the major expressers of EAAT2, a membrane-bound glutamate transporter that removes extracellular glutamate. On the other hand, CD45<sup>+</sup>, infiltrating immune (inflammatory) cells were the major expressers of xCT, a glutamate-cystein antiporter implicated in cancer previously. Data shown was from one cell sorting. Sortings were repeated three times, with similar results. Each cell sorting was performed by pooling multiple PNETs from one to two mice.

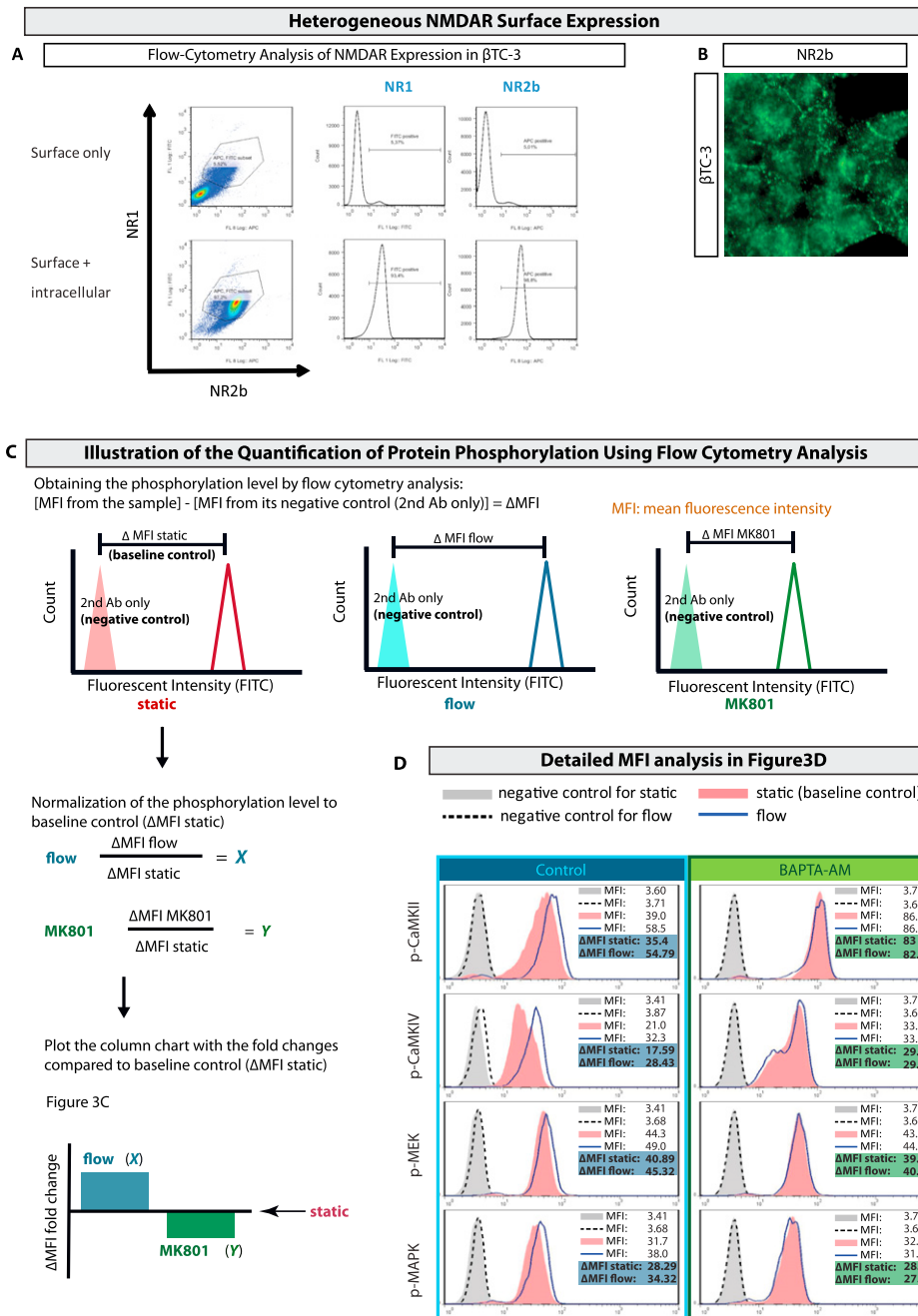


**Figure S5. Further Documentation of NMDAR Expression and Pathway Activity, Related to Figure 5**

(A)  $\beta$ TC-3 cells have a heterogeneous surface expression of NMDAR:

Staining for surface NMDAR subunits NR1 and NR2b identified two populations of  $\beta$ TC-3 cells in normal culture conditions, whereas the staining for total (both surface and intracellular) NMDARs showed a uniform population.

(B) The heterogeneous NR2b surface expression was also observed by immunocytochemistry staining.

(C) Illustration of the phosphoprotein analysis in static and flow conditions: to evaluate the interstitial flow-relevant change of protein phosphorylation, we included both negative control and baseline control in the flow cytometry analysis. The negative control (2<sup>nd</sup> antibody control) was to assess both the nonspecific binding of the 2<sup>nd</sup> antibody and the auto-fluorescence of the analyzed cells. The difference of mean fluorescence intensity (MFI) between each staining and its corresponding negative control ( $\Delta MFI$ ) represented the specific staining from the 1<sup>st</sup> antibody. The baseline control ( $\Delta MFI$  of the static condition) was intended to assess the basal level of protein phosphorylation of cells in 3D culture. We normalized the  $\Delta MFI$  of the flow and flow plus MK801 conditions to the baseline control, and plotted the ratio in each condition. The baseline control ( $\Delta MFI$  of the static condition) was set as 1 in the bar charts in Figure 5C.

(D) A detailed comparison of protein phosphorylation in control/BAPTA-AM-treated cells is shown. The different conditions didn't significantly change the auto-fluorescence of the cells, and the MFI of negative controls from different conditions had negligible differences, and thus are not shown in Figure 5D.

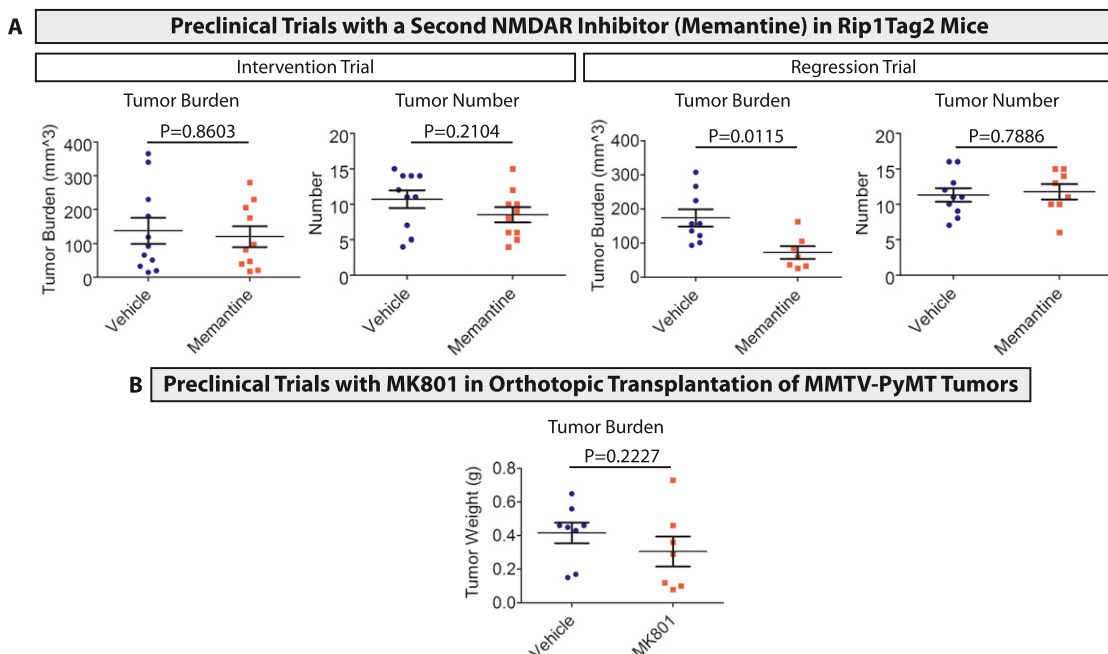


**Figure S6. Preclinical Trials with NMDAR Antagonists, Related to Figure 6**

(A) A preclinical trial was performed with a second NMDAR antagonist, memantine. The treatment was not effective in the intervention trial, but tumor burden was decreased in the regression trial. (The Mann-Whitney U test was performed) (Intervention trial:  $n = 10-11$  mice/group; regression trial:  $n = 8-11$  mice/group. The control group was the same data shown in Figure 6).

(B) A preclinical trial with MK801 was performed in MMTV-PyMT orthotopic transplantation model, following the same dosing regimen as for the PNET trials. The mice were sacrificed and tumors harvested after 3 weeks of treatment ( $n = 7-8$  tumors/four to five mice/group; some mice were bilaterally transplanted while others were unilaterally transplanted).

Data are represented as mean with SEM.



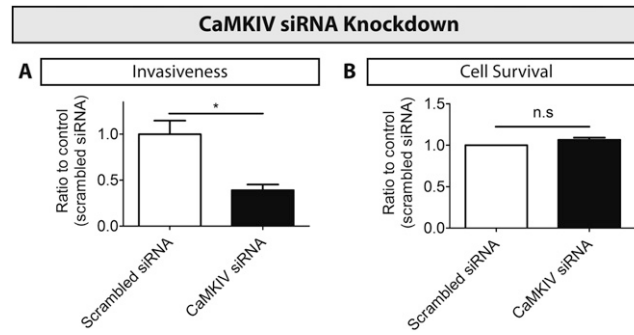


**Figure S7. CaMKIV Is Important for Flow-Guided Invasion, Related to Figure 7**

Knocking down CaMK-IV with siRNA reduced  $\beta$ TC3 invasiveness, thereby confirming the crucial involvement of CaMK pathway in tumor invasion (A). Cancer cell survival was not affected by the CaMKIV siRNA knockdown (B). Data are represented as mean with SEM.

**Table S1. Involvement of NMDAR Signaling in GEMMs—Summary of GEMMs Used, Related to Figure 1**

<b>GEMM</b>	<b>Onco-Genetic Modification</b>	<b>Samples Examined</b>	<b>Percentage of NR2b-positive Tumors</b>
<b>Pancreatic Neuroendocrine Tumor (PNET)</b>	Rip1Tag2	59 Tumors/9mice	94.9% (56 /59 Tumors)
<b>Breast Cancer</b>	MMTV-PyMT	8 Tissues / 6 mice	62.5% (5 /8 Tissues)
<b>Pancreatic Ductal Adenocarcinoma (PDAC)</b>	LSL-KrasG12D; p53Flox/WT; p48cre	3 Tissues / 3 mice	100% (12 /12 Tissues)
	LSL-KrasG12D; p53LSLR172H; p48cre	9 Tissues / 9 mice	

For the PNET GEMM, discrete tumors can be observed in pancreatic tissue sections. Therefore, NR2b expression was analyzed for individual tumors. In light of evident differential NR2b expression at the PNET center vs. margins, we only scored PNET margins to define positivity. In addition, although NR2b was differentially and heterogeneously expressed in PNET centers and margins, its expression pattern was relatively homogeneous locally (See Figure 1A), so we didn't need to manually determine the percentage of cells expressing NR2b. In brief, a PNET was considered positive for expression of NR2b if the staining at its margins was obviously positive compared to 2<sup>nd</sup> antibody-only control staining. (The same criteria was applied to both human and mouse samples. See Figure 2A for the intensity definition, in which low, intermediate and high are all considered to be positive.)

For the breast cancer and PDAC GEMMs, merged lesions of varying tumor grades were noted on the tissue sections, thus we were not able to analyze the expression for each tumor. Therefore, positive NR2b expression is defined as "Positive staining in >5% of cancer cells on the whole tissues section". The definition is similar to the intensity score of ER/PR expression in breast cancer samples, in which only the staining of tumor cells, but not their normal tissue counterparts, was taken into account (Harvey et al.,

1999; Onitilo et al., 2009), as normal breast tissues could also express ER/PR (van Agthoven et al., 1994), but ER/PR on tumor cells are still prognostically important (Harvey et al., 1999).

**Table S2. Involvement of NMDAR Signaling in Human Cancers—Summary of TMA Findings, Related to Figure 2**

<b>Human TMA (catalogue number)</b>	<b>Samples Examined</b>	<b>Percentage of NR2b-positive tumor samples</b>
<b>Ovarian Cancer (OV241a)</b>	12 samples / 6 patients	50%
<b>Pancreatic Cancer (PA481)</b>	24 samples / 12 patients	100%
<b>Breast Cancer (BRC961)</b>	63 samples / 34 patients	92.1%
<b>Glioma (GL241a)</b>	20 samples / 10 patient	40%
<b>Prostate Cancer (PR481)</b>	24 samples / 12 patients	0%

Positive staining is defined as >5% of cancer cells with evident NR2b staining, regardless of staining intensity, the same criteria as the analysis of PDAC and breast cancer GEMMs (see Supplementary Table 1). (Also see Figure 2A, in which low, intermediate and high are all considered to be positive). “Positive NR2b staining percentage” thus indicates the fraction of patient samples analyzed on a TMA whose tumors, according to this criterion, were judged to contain cancer cells positive for NR2b staining.

**Table S3. Human Cancer Cell Lines Used to Assess Invasion and NMDAR Signaling, Related to Figure 3**

<b>Cancer Types</b>	<b>Cell-line</b>	<b>Subtype</b>	<b>Clinical Subtype</b>
<b>Breast Cancer (Heiser et al., 2012)</b>	MCF-7	Luminal	ER/PR Positive
	MDA-MB-453		
	SKBR3	ERBB2	HER2/ERBB2
	HCC1954		
	HCC1806	Basal	Triple Negative
	BT549	Claudin-Low	
	HCC38		
	HCC1395		
<b>Pancreatic Ductal Adenocarcinoma (Collisson et al., 2011)</b>	SUIT2	Classical	
	BxPC3		
	HPAF_II		
	3.27	Quasi-Mesenchymal	
	DanG		

**Table S4. List of qRT-PCR (Taqman) Probes Used in This Study, Related to Extended Experimental Procedures “mRNA reverse transcription and quantitative real time PCR (Q-PCR)”**

<b>Species</b>	<b>Gene Name</b>	<b>Gene Symbol</b>	<b>Taqman Probes</b>
<b>Human</b>	Rpl14 (reference gene)	<i>Rpl14</i>	Hs03004339_g1
	NR1	<i>Grin1</i>	Hs00609557_m1
	NR2a	<i>Grin2a</i>	Hs00168219_m1
	NR2b	<i>Grin2b</i>	Hs00168230_m1
<b>Mouse</b>	Rpl19 (reference gene)	<i>Rpl19</i>	Mm02601633_g1
	NR1	<i>Grin1</i>	Mm00433790_m1
	NR2b	<i>Grin2b</i>	Mm00433820_m1
	vGlut1	<i>Slc17a7</i>	Mm00812886_m1
	vGlut2	<i>Slc17a6</i>	Mm00499876_m1
	vGlut3	<i>Slc17a8</i>	Mm00805413_m1
	EAAT2	<i>Slc1a2</i>	Mm00441457_m1
	xCT	<i>Slc7a11</i>	Mm00442530_m1